1 OF 1
AD A
104687

(12)

AD A104687

REPORT DOCUMENTATION PAGE		READ INSTRUCTIONS BEFORE COMPLETING FORM
1. REPORT NUMBER GALCIT-SM-81-7	2. GOVT ACCESSION NO. AD-A104 687	3. RECIPIENT'S CATALOG NUMBER
4. TITLE (and Subtitle) DYNAMIC FRACTURE IN VISCOELASTIC SOLIDS.		5. TYPE OF REPORT & PERIOD COVERED Annual Report 1/1/81 - 8/31/81
		6. PERFORMING ORG. REPORT NUMBER
7. AUTHOR(s) K.S. Kim, W.G. Knauss		8. CONTRACT OR GRANT NUMBER(s) ONR N00014-78-C-0634
9. PERFORMING ORGANIZATION NAME AND ADDRESS California Institute of Technology 105-50 Pasadena, CA 91125		10. PROGRAM ELEMENT, PROJECT, TASK AREA & WORK UNIT NUMBERS
11. CONTROLLING OFFICE NAME AND ADDRESS Office of Naval Research, Code 473 Dept. of the Navy, Arlington, VA 22217		12. REPORT DATE July 2, 1981
		13. NUMBER OF PAGES 86
14. MONITORING AGENCY NAME & ADDRESS(If different from Controlling Office) LEVEL		15. SECURITY CLASS. (of this report) UNCLASSIFIED
		15a. DECLASSIFICATION/DOWNGRADING SCHEDULE

16. DISTRIBUTION STATEMENT (of this Report)

Approved for public release; distribution unlimited.

17. DISTRIBUTION STATEMENT (of the abstract entered in Block 20, if different from Report)

DTIC
ELECTE
SEP 29 1981
H

18. SUPPLEMENTARY NOTES

19. KEY WORDS (Continue on reverse side if necessary and identify by block number)

Dynamic fracture, viscoelasticity, running cracks, crack branching.

20. ABSTRACT (Continue on reverse side if necessary and identify by block number)

Dynamic crack propagation in viscoelastic media is studied experimentally with, Homalite 100, and a polyurethane, Solithane 113, at various temperatures. Employing the method of caustics, high speed photography determines the variation of

DD FORM 1473
1 JAN 73

81 9 28 164

DTIC FILE COPY

the stress intensity factor and the velocity of a running
crack initiated and driven by the dynamic step loading on
the faces of an initial semi-infinite track in an infinite
medium. The method of caustics is extended for time
dependent stress intensity factors of running cracks in
viscoelastic materials. Also, the viscoelastic effects on
the initiation of a running crack, the variation of the
stress intensity factor, the speed of the crack and the
branching of the running crack are discussed. A mechanism
of branching is proposed based on the study of the fracture
surfaces.

Accession For
NTIS
DTIC
J

by
Dist

A

SM 81-7

Annual Report on

DYNAMIC FRACTURE IN VISCOELASTIC SOLIDS

by

K. S. Kim

W.G. Knauss

July 2, 1981

Table of Contents

ABSTRACT

Dynamic crack propagation in viscoelastic media is studied experimentally with a polyester known as Homalite 100 and a polyurethane known as Solithane 113 at various temperatures. Employing the optical method of caustics [1-5], high speed photography is used to determine the variation of the stress intensity factor and the velocity of a running crack initiated and driven by the dynamic step loading on the faces of an initial semi-infinite track in an infinite medium. The loading condition is simulated experimentally with the technique introduced by Smith and Knauss [6]. In this work an application of the method of caustics is extended for the determination of the time dependent stress intensity factor of a running crack in a viscoelastic material. Also, the viscoelastic effects on the initiation of a running crack, the variation of the stress intensity factor, the speed of the crack and the branching of the running crack are discussed. In addition, a mechanism of branching is proposed based on the study of the fracture surfaces.

1 INTRODUCTION

When one compares the progress made in understanding quasi-static fracture with that related to dynamic crack propagation one is impressed with the wide range of engineering applications in which quasistatic fracture analyses have proven useful. Speaking comparatively, much less understanding has been generated for dynamics related problems. No doubt it is primarily a matter of time before a body of knowledge on dynamic fracture has been developed that has a design oriented impact comparable to that which is now offered with respect to quasi-static fracture.

The problem of dynamic fracture in viscoelastic solids has enjoyed a proportionately still smaller degree of attention. This is in part due to the fact that a) viscoelastic solids are relative newcomers on the engineering scene, b) analytical treatment of dynamics problems is significantly more difficult than for purely elastic materials and c) interpretation of experimental work is severely limited by the lack of analytical understanding.

Because of this relative paucity of effort in dynamic fracture, there appears to have emerged in recent years several attempts to improve our empirical knowledge of dynamic fracture. However, these new developments are almost exclusively devoted to the fracture of rate insensitive materials. While experimentation proceeds with polymeric solids as test materials these polymers

are chosen as metal substitutes primarily for reason of convenience; their viscoelastic behavior tends to be an undesirable inconvenience rather than a chosen characteristic.

This report outlines work conducted to better define and predict the friability of strongly viscoelastic solids, and oriented to better understand the effects of viscoelastic material behavior on the fracture process with particular attention devoted to comminution related problems. The motivation for this work derives from problems encountered in understanding safety limitations in handling the new high energy solid propellants (vulnerability) as well as the problem of deflagration-to-detonation transition (DDT). Both phenomena depend potentially strongly on the rapid generation of large amounts of new (burning) surface such as is observed to occur usually in dynamic fracture processes. The time scale of dynamic fractures is typically in the high microsecond range (hundreds of μsec) and thus of the same order experienced in a motor DDT.

The basic interest here is to understand the conditions that lead to crack branching. For, if crack branching criteria can be established one would, in principle, be able to estimate whether the dynamic stresses accompanying DDT could cause a rapid proliferation of crack surface via branching and thus feed the DDT process by offering a rapidly growing burning surface.

There are several important issues that are subordinate to this basic question:

a) Wave propagation in viscoelastic solids: Simple problems of wave propagation involving viscoelastic material behavior are fairly well understood; so is the attenuation of propagating waves in simple geometries. However, in geometries involving cracks or even propagating cracks much less is known. It is hoped that work going on at this time at other institutions can usefully complement the present effort in the future. Of particular interest would be information on the crack tip strain field of a running crack.

b) A problem similar and related to that just mentioned under a) is the experimental identification of the crack tip stresses. To date this has been accomplished via optical caustics, although a slightly more laborious method, namely photoelasticity, could be employed. In either case the modification enforced by viscoelastic material behavior offers a major complication. To date we have assumed in part of our work employing caustics that a modicum of viscoelastic behavior does not materially effect the caustics, so that the crack tip stresses are approximately determined by the caustics as interpreted via linear elasticity. For other parts of our investigation concerned with a stronger viscous material component that assumption is not justified and ad hoc modifications are used as indicated later on in this report.

c) Probably an important consideration in any explanation or theory for multiple crack branching is the microstructural response of the material at the crack tip. To date little attention has been paid to this fact, in part because virtually no

information exists on its likely effect. As a consequence we report here some detailed, if initial information on how the material responds as crack branching is approached.

d) With this problem of micro structural effects is connected the general question of constitutive behavior of viscoelastic propellant materials under high rates of loading. That behavior is fairly well understood, as far as engineering accuracy is concerned as long as (strain) loading rates are below, say, 1000/sec. However, when rates 1000 times higher are involved time-temperature superposition is somewhat questionable without some further tests.

2 BRIEF EXPERIMENTAL REVIEW

In this work the fracture of viscoelastic polymers under dynamic loading is studied. The loading condition is a step loading on the faces of a semi-infinite crack in an unbounded visco-elastic two-dimensional plane. The condition is simulated experimentally by applying on the crack faces electromagnetic forces induced by a square pulse of high electric current flowing in opposite directions through a doubled up thin copper strip; this strip, the legs of which are separated by a Mylar insulator 125 μm thick, is inserted into the crack of a large specimen plate. In order to control the intrinsic time scale of viscoelasticity, the

temperature is changed through the use of the time-temperature shift phenomenon. In these experiments, Homalite-100 is used at three different temperatures (60°C, 80°C, 100°C) under three different load levels. Solithane 113 (50/50) is also used in a similar fashion. (0°C, -20°C, -40°C, -60°C.)

The result of this study is basically divided into three parts. The first part is the characterization of the stress state near the crack tip, measuring the stress intensity factor K(t) as a function of time in the given load history. This is done experimentally by extending the method of caustics to viscoelastic materials. This extension is discussed in detail in the following sections [4,5,6]. For a qualitative comparison, the stress analysis is also performed analytically for the case of a stationary crack in antiplane shear (mode III) deformation within the realm of linear viscoelasticity. Also discussions of elastic analyses [7-16] and viscoelastic analysis [17,18] for the moving crack are mentioned.

The second part of this report concerns the process of fracture under the characterized stress state at the crack tip. This is investigated by relating the stress intensity factor and the corresponding velocity of the extending crack, and by observing the fracture surfaces microscopically. Together with the data of crack velocities at various temperatures, data for the initiation of a running crack are obtained. In addition it appears to turn out that the micromechanism of crack propagation is related to the stability of the crack front in the fracture

surface plane; this behavior may be interpreted to produce discontinuous crack growth with the attendant generation of rough surfaces.

In the third part of this report we make some observations on the behavior of crack branching. In this work a possible mechanism of crack branching is suggested, which may explain the continuous energy release rate before and after branching. Observations seem to show that the branching is preceeded by the sequence of (i) division of crack front in the fracture surface plane, (ii) deviation of each of the new crack fronts from the original fracture surface plane due to crack path instability, and (iii) interaction of the deviated crack fronts which would cause further global branching depending on the stress state near the global crack front and finally (iv) helical climbing of the crack front and subsequent side cutting. Details of this mechanism are given in section 7 with the picture of fracture surfaces near the place where the crack branching occurred.

For further study, more effort has to be expended in obtaining analytical results for the transient behavior of running cracks in viscoelastic media under dynamic loading. Also, analytic modelling of the instability of the crack front has to be improved. Finally, since irreversible heat dissipation is important in the process of viscoelastic fracture, thermodynamic considerations need to be examined for the study of the energy balance by measuring other physical quantities such as the

temperature rise at the running crack tip.

3 ANALYSES OF VISCOELASTIC DYNAMIC FRACTURE

In preparation for the experiments described later on we
consider now the analyses of dynamically loaded cracks in a two
dimensional domain. The appropriate geometry is shown in fig. 1.
For the purposes of this analysis we consider that the dynamic
loading is achieved in step fashion and is applied to the faces
of the semi-infinite crack embedded in the unbounded medium. From
a practical point of view, this problem is appropriate for our
later experiments as long as the plate dimensions used in the
experiments are so large, that during the course of the experiment
no reflected waves from the boundary arrive back at the (moving)
crack tip. In terms of the linear analyses employed subsequently
the stresses near the crack tip can be characterized by the
singularity expansion which is characterized in part, by the
stress intensity factor. This stress intensity factor varies as
a function of the load history and as a function of the crack tip
velocity. For dynamic linearly elastic problems in the plane the
analytical tools have been well developed by Achenbach and
Freund [11-16]. As a result of these analyses it is well known that
the dynamic stress intensity factor can be expressed in the form

$$K[\ell(t),\dot{\ell}(t)] = k[\dot{\ell}(t)]K[\ell(t),0] \qquad (1)$$

In this expression $\ell(t)$ denotes the instantaneous crack length
and the dot connotes differentiation with respect to time. Note
that this stress intensity factor is of a product form, in which
the second factor is the stress intensity factor corresponding
to the corresponding <u>static</u> problem and the first factor is a
function of the instantaneous crack speed only. We observe also
that the static stress intensity factor can be computed from

$$K[\ell(t),0] = \int_0^\infty \int_{-\infty}^t K_F(\chi, t-\xi) \; \frac{P(\chi,\xi)}{\partial \xi} \; d\xi \; d\chi \qquad (2)$$

where $K_F(\chi,t)$ is a Green's function solution for the stress
intensity factor of a stationary crack, to the surface of which a
delta function has been applied in step fashion; ξ denotes the
distance parameter along the crack length measured from the tip
and P is the distributed pressure which is a function of this
distance parameter χ as well as a function of time ξ.

When viscoelasticity is involved the solution indicated in
equation (1) is no longer valid; it turns out that for even
stationary cracks the stress intensity factor resulting from the
fundamental solution of a Dirac delta function to the crack
surfaces is not available; in other words, the function $K_F(\chi, t-\xi)$
is not known at this time. Because this general tool of computing
dynamic stress intensity factors for linearly elastic problems
does not have a counter-part in viscoelasticity, there appear to
be at this time only a few solutions to problems available in

which special boundary conditions have been imposed and in which
rather special constitutive relations are used. For example,
Atkinson and List [17] solved an antiplane shear problem (mode III)
in which loading was applied as a step function in time, and in
which the viscoelastic material was represented as a standard
linear solid. Moreover, in this problem the crack was considered
to move with a constant velocity which starts instantaneously at
time zero and the loading follows the moving crack. This physical
situation would correspond to an instantaneously applied gas
pressure which can spread with the same velocity with which the
crack propagates. In spite of the simplicity of the physical
problem and inspite of the limitations in the applicability of
these results* later experimental problems it is interesting to
extract from this analysis the following observation: If the
velocity of a crack is sufficiently high then for large time
after the crack starts to grow the stress intensity factor
approaches a constant value; this constant value depends on the
crack tip velocity v for the condition $\frac{v}{c} > \frac{\alpha}{\beta}$* where c $= \sqrt{\mu/\rho}$.
We further extract from this solution that the change of this
stress intensity factor for very short times after the step
loading has been accomplished is also given by the elastic
solution. This is even true if the material is represented by a
Maxwell model.

---

* This problem is considered for the special constitutive equation
  suggested by Achenbach and Chao [19]

$$(\frac{d}{dt} + \beta)^2 \sigma = 2\mu (\frac{d}{dt} + \alpha)^2 \epsilon ; \tag{3}$$

Observe now that we are interested in short term behavior in our later experiments; in particular we are interested in the fracture of viscoelastic materials that may approach brittle fracture in non-viscoelastic materials. For this reason we carry out first the subsequent analyses for dynamic loading on the crack faces, allowing, however, the crack to remain stationary in the linearly viscoelastic solid. Because we are dealing with a semi-infinite crack in the infinite domain there is no characteristic length in this formulation. For this reason it turns out that even for a linearly viscoelastic material the Laplace transformed solution can be manipulated with the aid of the Wiener-Hopf technique. Thereafter the solution procedure is basically the same as for the linearly elastic case. The difficulty arises thereafter, because it is still necessary to determine the inverse Laplace transform which in the elastic case is carried out most easily in terms of the Cagniard-Hoop [20] method. In the viscoelastic case this method cannot be exercised because it is extremely difficult to define the double inversion variable consisting of the spacial variable y and the time variable t. Instead we perform a single inversion on the spacial variable y to leave a solution that depends on the time-time like Laplace variable s.

Consider the semi-infinite crack under shear loading as shown inset in figure 2a. The shear stress

$$\sigma_{yz} = -\tau H(t) \qquad (4)$$

is applied to the crack surfaces embedded in the infinite domain, the motion of which is governed by the single, non-trivial equation of motion

$$\sigma_{yz,y} + \sigma_{xz,x} - \rho\dot{w} = 0 \tag{5}$$

where w is the velocity component in z direction, augmented by the strain displacement compatibility conditions and stress-strain relations ($\mu(t)$ = relaxation modulus in shear)

$$\frac{\partial w}{\partial x} = \frac{\partial \epsilon_{xz}}{\partial t} \quad , \quad \frac{\partial w}{\partial y} = \frac{\partial \epsilon_{yz}}{\partial t} \tag{6}$$

$$\sigma_{xz} = \int_0^t \mu(t-\xi)\frac{\partial \epsilon_{xz}}{\partial \xi} \, d\xi = \int_0^t \mu(t-\xi)\frac{\partial w}{\partial y} \, d\xi \tag{7a}$$

$$\sigma_{yz} = \int_0^t \mu(t-\xi) \frac{\partial \epsilon_{yz}}{\partial \xi} \, d\xi = \int_0^t (t-\xi)\frac{\partial w}{\partial y} \, d\xi \tag{7b}$$

Upon Laplace transforming these equations we have

$$\bar{\sigma}_{yz,y} + \bar{\sigma}_{xz,x} - \rho s\bar{w} = 0 \tag{8}$$

$$\bar{\sigma}_{xz} = \bar{\mu}(s)\frac{\partial \bar{w}}{\partial x} \tag{9a}$$

$$\bar{\sigma}_{yz} = \bar{\mu}(s)\frac{\partial \bar{w}}{\partial y}$$

which equations combine to render the field equation for $\bar{w}$

$$\nabla^2\bar{w} - \frac{\rho s}{\bar{\mu}} \bar{w} = 0 \tag{10}$$

with the attendant boundary conditions

$$\bar{\sigma}_{yz}(x,o;s) = \bar{\mu}(s)\frac{\partial \bar{w}}{\partial y} = -\frac{\tau}{s} \; ; \; x < 0 \qquad (11)$$

$$\bar{w}(x,o;s) = 0 \qquad\qquad x > 0 \qquad (12)$$

Apply now the two-sided Laplace transform to $\bar{w}$ with respect to "x" resulting in

$$\hat{\bar{w}}(\eta,y;s) = \int_{-\infty}^{\infty} \bar{w}(x,y;s) e^{-\gamma \eta x} \, dx \qquad (13)$$

where $\gamma = \sqrt{\rho s/\bar{\mu}}$. Equation (10) becomes then

$$\frac{d^2 \hat{\bar{w}}}{dy^2} - \gamma^2(1 - \eta^2)\hat{\bar{w}} = 0 \qquad (14)$$

with the solution (vanishing at $y \to \infty$)

$$\hat{\bar{w}} = A(\eta,s)e^{-\gamma \zeta y}; \qquad \zeta = \sqrt{1 - \zeta^2} \qquad \text{Re} \geq 0 \qquad (15)$$

Evaluation of the boundary conditions (11) and (12), suitably transformed, yields

$$\hat{\bar{w}}(\eta,o;s) = \int_{-\infty}^{0} \bar{w}(x,o;s) e^{-\gamma \eta x} \, dx \qquad (16)$$

$$= F_{-}(\eta;s) = A(\eta;s)$$

which is analytic for Re $\eta < 0$.

$$\sigma_{yz}(\eta,o;s) = \int_{-\infty}^{0} - \frac{\tau}{s} e^{-\gamma \eta x} \, dx + \int_{0}^{\infty} \overline{\gamma}(x,o,s) e^{-\gamma \eta x} \, dx$$

$$= \frac{\tau}{\gamma \eta s} + F_{+}(\eta;s) \tag{17}$$

$$= \overline{\mu} \left. \frac{\partial \widehat{w}}{\partial y} \right|_{y=0} = - \overline{\mu} \gamma \zeta A(\eta;s)$$

where $F_{+}(\eta,s)$ is analytic for Re $\eta > -1$. Thus, upon eliminating $A(\eta;s)$ from (16) and (17)

$$F_{+}(\eta;s) = - \overline{\mu} \gamma \zeta F_{-} - \frac{\tau}{\gamma \eta s} \tag{18}$$

We apply now the Wiener-Hopf technique after writing (18) as

$$\frac{F_{+}}{\zeta_{+}} + \frac{\tau}{\gamma s \eta} \left[\frac{1}{\zeta_{+}} - \frac{1}{\zeta_{+}(0)} \right] = - \overline{\mu} \gamma \zeta_{-} F_{-} - \frac{\tau}{\gamma s \eta \zeta_{+}(0)} \tag{19}$$

where $\zeta = \zeta_{+} \zeta_{-}$ and $\zeta_{+} = (1+\eta)^{\frac{1}{2}}$; $\zeta_{-} = (1-\eta)^{\frac{1}{2}}$ and $\zeta_{\pm}(0)$ are the appropriate limits of ζ_{+} and ζ_{-} as $\eta \to 0$.

Considering $\eta \to \pm\infty$ it follows from the fact that the left side and right side of (19) are entire functions in their respective half planes and vanish there one has

$$- \overline{\mu} \gamma \zeta_{-} F_{-} - \frac{\tau}{\gamma s \eta \zeta_{+}(0)} = 0 \tag{20}$$

or

$$A(s,\eta) = F_{-} = - \frac{\tau}{\overline{\mu} \gamma^{2} s \eta \zeta_{+}(0) \zeta_{-}} \tag{21}$$

The inverse of 16 yields then

$$\bar{w}(x,y;s) = - \frac{\tau}{\bar{\mu}\gamma^2 s \zeta_+(0) 2\pi i} \int_{Br} \frac{e^{\gamma(\eta x - \zeta y)}}{\eta_-(\eta)} \, d(\eta\zeta) \qquad (22)$$

$$= - \frac{\tau}{\bar{\mu}\gamma s 2\pi i} \int_{Br} \frac{e^{\gamma(\eta x - \zeta y)}}{\eta(1-\eta)^{\frac{1}{2}}} \, d\eta$$

and from (17)

$$\bar{\sigma}_{yz}(x,y;s) = \bar{\mu} \frac{\partial \bar{w}}{\partial y} = \frac{\tau}{2\pi i s} \int_{Br} \frac{\beta e^{\gamma(\eta x - \zeta y)}}{\eta(1-\eta)^{\frac{1}{2}}} \qquad (23)$$

Here Br denotes the Bromwich integration
contour shown in the sketch.

Upon applying the Cagniard-Hoop
transformation one finds for $y = 0$.
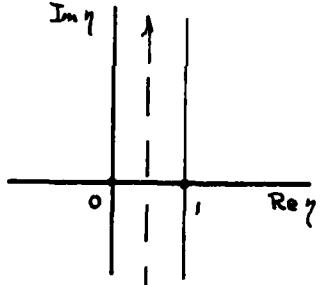
$$\bar{\sigma}_{yz}(x,o;s) = \frac{\tau}{\pi s \sqrt{x}} \int_0^\infty \frac{\sqrt{\xi}}{\xi + x} e^{-\gamma(\xi + x)} \, d\xi \qquad (24)$$

from which it follows that the Laplace transform of the stress
intensity factor (with respect to time) is

$$\bar{K} = \lim_{x \to 0} \sqrt{2\pi x} \, \bar{\sigma}_{yz} = \frac{2}{\pi} \frac{\tau}{s} \int_0^\infty \frac{e^{-\gamma\xi}}{\sqrt{\xi}} \, d\xi \qquad (25)$$

$$= \sqrt{\frac{2}{\gamma}} \frac{\tau}{s} = \sqrt{\frac{2\sqrt{\mu}}{\sqrt{\rho s}}} \, \frac{\tau}{s}$$

In general this inversion needs to be carried out numerically. However, for illustrative purposes we turn now to an evaluation of this relation for a (viscoelastic) Maxwell solid, for which

$$\mu(t) = \mu_0 \exp(-\frac{\mu_0}{\eta_0} t) \tag{26}$$

with μ_0 and η_0 being material constants. One has therefore

$$\bar{\mu}(s) = \frac{\mu_0}{\frac{\mu_0}{\eta_0} + s}$$

so that (25) becomes, with $c_t^0 = \sqrt{\mu_0/\rho}$

$$\bar{K} = \sqrt{2} c_t^0 \, \tau \, \frac{1}{s[s(\frac{\mu_0}{\eta_0} + s)]^{\frac{1}{4}}} \tag{27}$$

The inversion of (27) can be accomplished in terms of a convolution integral to yield (Γ = Gamma function)

$$K(t) = \frac{\tau \sqrt{2} c_t^0}{\Gamma(\frac{5}{4}) \Gamma(\frac{1}{4})} \int_0^t \xi^{-\frac{3}{4}} (t-\xi)^{\frac{1}{4}} e^{-\frac{\mu_0}{\eta_0}\xi} \, d\xi \tag{28}$$

In non-dimensional form this becomes, with $\kappa = \frac{\mu_0}{\eta_0} t$,

$$\frac{K(t)}{\tau \sqrt{\frac{\eta_0 c_t^0}{\mu_0}}} = \frac{2 \cdot \kappa}{\Gamma(\frac{5}{4}) \Gamma(\frac{1}{4})} \int_0^1 p^{-\frac{3}{4}} (1-p)^{\frac{1}{4}} e^{-\kappa p} \, dp \tag{29}$$

$$\simeq 2\sqrt{\frac{2\kappa}{\pi}} \qquad \kappa \ll 1$$

$$\simeq \frac{\sqrt{2}}{\Gamma(\frac{5}{4})} \kappa^{\frac{1}{4}} \qquad \kappa \gg 1$$

The results, obtained, numerically from (29) are shown in
figures 2a and b.

4 EVALUATION OF THE STRESS INTENSITY FACTOR -
   EXPERIMENTAL PRELIMININARIES

In experimental stress analyses relating to static or
dynamic cracks, there are generally two techniques that have
evolved during the past decades to measure stress intensity
factors. The most recent development in that direction has been
the method of caustics which is the one that is adopted in this
work. The somewhat older and more classical method is based on
photoelasticity. Either method has been employed to date primarily
to elastic materials. This is unequivocally true with respect to
dynamic problems. It turns out that the photoelastic method has
certain disadvantages for our investigation: Most important among
these restrictions is that the Homelite 100 material with which
we are working in a part of this investigation, is used in
relatively thin sheets (3/16 inch thick) and the fringe count
is not sufficiently high to give a reasonable number of fringes
in these tests. There are a number of fringe multiplication
techniques available; however, they require a large amount of
light which is not available in our set-up but which is required
for the very high speed photography used here. Apart from these
limitations arising from the specimen size and from the experimental
equipment it turns out that the fringe interpretation-through

fitting an analytical expression in a least square fit- has
probably no greater accuracy than the limitations inherent in
the caustic method. Beyond this comparison it turns out that
the caustic method is well suited to our optical setup allowing
sufficient passage of light in a single pass from the laser light
source to expose the film during the 20 nano second exposure
required for stop action at 100,000   frames/sec as employed in
these tests. Moreover in some of our tests (on Solithane 113) the
rigidity of the test material is relatively small. As a consequence
somewhat larger than "normal" deformations occur which cause a
relatively large deflection of the light beam. As a result, it is
difficult to capture all this information with a reasonably
sized lense. In contrast the caustic method exhibits many fewer diffi-
culties   and is relatively simple to apply. For this reason we
extend here the computations underlying the shape of the caustic
in elastic materials to viscoelastic fracture.

 For reference purposes consider the optical set-up shown
in figure 3. Denote a generic point in the crack tip vicinity by
$\underline{x}$ and consider a light ray passing through this point $\underline{x}$ in the
loaded specimen. In the image plane the ray strikes the corresponding
point $\underline{x}'$ so that we have the transformation

$$\underline{x}' = \underline{x} + \underline{\omega}(\underline{x},t) \tag{30}$$

where we denote by $\underline{\omega}$ the deflection vector due to the stress
state near the crack tip. This deflection vector can be expressed

as [3]

$$\underline{\omega}(\underline{x},t) = z_0 \cdot \text{grad } \Delta s(\underline{x},t) \tag{31}$$

where z_0 is the distance between the stress specimen midplane
and the image plane and Δs is the change of the effective optical
path length

$$\Delta s = d_0 C * \{\sigma_I + \sigma_{II} \pm \lambda(\sigma_I - \sigma_{II})\} . \tag{32}$$

This change of the optical path length depends on the principal
stresses at the point $\underline{x}$, on the specimen thickness d_0 and on a
constant C (a shadow optical constant). If the material is
optically anisotropic a parameter λ will enter into the relation
between the optical path length change and the state of stress.
For optically isotropic materials this constant or anisotropy
function is zero. For a viscoelastic material the optical path
length is a function of the stress history. Expressed mathematically
for a linearly viscoelastic system the path length difference is a
convolution with the stress state and the shadow optical function
$C(t)$. For isotropic linearly viscoelastic material we have
therefore, instead of eq. (32),

$$\Delta s = d_0 C * \sigma \tag{33}$$

where we have written σ for the first stress invariant (sum of
the principal stresses) and allowed for isotropc behavior only.
Using these stress representations in the immediate vicinity of
the crack tip for which [21,22] with mode I stress intensity
factor K_I,

$$\sigma = K_I \sqrt{\frac{2}{\pi r}} \cos\frac{\theta}{2} + a \tag{34}$$

where $r = \sqrt{x_1^2 + x_2^2}$, $\theta = \tan^{-1}\frac{x_2}{x_1}$ and "a" is a constant. Making use of equations (30), (31), (33) and (34) there results

$$\underline{x}' = \underline{x} + d_o z_o (C*K_I) \; \mathrm{grad}(\sqrt{\frac{2}{\pi r}}\cos\frac{\theta}{2}) \tag{35}$$

Employing now the condition that the Jacobian vanishes, that is

$$J = \frac{\partial(x_1', x_2')}{\partial(x_1, x_2)} = 0$$

one obtains for the shape equation of caustics the relation

$$r = (\frac{3z_o d_o}{2\sqrt{2\pi}}C*K_I)^{\frac{2}{5}}$$

or

$$K_I = \frac{2\sqrt{2\pi}}{3z_o d_o} \; |C^{-1}|*r^{\frac{5}{2}} \tag{36}$$

This equation is, strictly speaking, true only for a stationary crack and it is therefore used later on for the variation in the stress intensity factor of a stationary crack (see section 5). We now turn the measurement of the shadow optical function $C(t)$. Clearly the function $C(t)$ is of primary importance in the experimental evaluation of stress intensity factors in visco-elastic materials.

5 THE CAUSTIC FOR A STATIONARY CRACK IN A VISCOELASTIC MATERIAL

Equation (36) may be rewritten upon using equation (30), (31) and (33) to yield

$$K_I = \frac{\sqrt{2\pi}}{3f^{\frac{5}{2}}z_o d_o} \; |C^{-1}| * D_o^{\frac{5}{2}} \tag{37}$$

In this latter form D_o denotes the diameter across the caustic in the y-direction. The shadow optical function C is composed of two contributions. One arises from the change of the index of refraction, (denote this contribution by A) and by the lense like deformation of the viscoelastic sheet and; this contribution is given by $(n-1)\frac{\nu}{E(t)}$ so that C may be defined as

$$C = A - (n - 1)\frac{\nu}{E} \tag{38}$$

Let us assume now that the contribution (optical relaxation) to a change in the index of refraction is small and proportional to mechanical relaxation, say, $\epsilon \cdot \frac{\nu}{E}$ [23,24]; then C is given only by the rigidity contribution

$$C = (1 - n + \epsilon)\frac{\nu}{E} \tag{39}$$

which allows us to write (37) as

$$(1 - n + \epsilon)\frac{3z_o d_o}{\sqrt{2\pi}}(\frac{\nu}{E} * K_I) = \{\frac{D_o}{\epsilon}\}^{\frac{5}{2}}$$

Clearly this equation indicates that if a stress intensity factor of known magnitude acts at the tip of the crack, then the caustic

diameter D_o should grow in conformity with the shadow optic function $C(t)$. Moreover, this shadow optic function should be directly proportional to the creep compliance - or at worst a convolution of a creep compliance and Poisson's ratio - in accordance with equation (39).

In order to test out this relation it is appropriate to make use of the viscoelastic properties of Solithane 113 and device a geometry with a non-propagating crack. Such a geometries is given by a large sheet with a central crack perforation. The stress intensity factor for this problem remains constant if a step function as the far field stress is applied. In fig. 4a and b we show a sequence of time exposures of a caustic at the tips of such a crack in Solithane 113. These particular figures were taken at -10 and $-15^{o}C$; clearly the diameter of the caustic is seen to grow with time after load application. This type of data is then obtained at three different temperatures and the results suitably normalized are shown in figure 5. Also shown in that figure is the reciprocal Young's relaxation modulus normalized by its value at infinite time-that is, by its rubbery modulus. This function is taken as an approximation to the creep compliance in uniaxial tension. It is seen that the comparison of the analytical estimate is quite reasonable with the data derived from tests. The data derived from these three temperatures has been superposed according to the time temperature shift phenomenon making use of the shift factor which has been determined previously for Solithane-113 [25].

In figure 6 the shadow optical function for Homalite 100 is given reduced to a temperature of $60^{\circ}C$ [24]. This curve is the result of tests at temperatures of 60, 80 and $100^{\circ}C$ with an estimated scatter band as indicated by the error bar.

Both curves for the shadow optical functions are basic input into the experimental determination of the stress intensity factor for running cracks: The shape and size of the caustic involves a convolution of this property with the deformation history at the tip of the moving crack tip. We proceed to discuss now this analytical problem.

6 ANALYTICAL DETERMINATION OF THE CAUSTICS FOR A CRACK MOVING IN A VISCOELASTIC SOLID

We need to recall that analyses of the dynamic stress intensity factor for a moving crack tip are usually formulated so that the state variables such as stress, strain etc. are expressed in terms of a position vector $\underline{x}$ which has its origin at the running crack tip. In contrast the shadow optic function $C(t)$ is a material property and therefore the appropriate convolution "$*$" has to be applied with respect to a fixed material point $\underline{X}$ in equation (32). Accordingly the expression for the optical path length which is commensurate with equation (32) is given by

$$\Delta s = d_0 \int_{-\infty}^{t} C(t-\tau) \left(-v\frac{\partial \sigma}{\partial x_1} + \frac{\partial \sigma}{\partial \tau} \right)\bigg|_{\underline{X}} d\tau \qquad (40)$$

where v is the velocity of the crack tip and it is assumed that the crack propagates in the x_1 direction. An illustrative trajectory of the material path in the t-x_1 plane is shown in figure 7.

Let us now turn to consider an approximation for the caustic in a viscoelastic material arising from a crack tip moving through a two dimensional geometry. We consider this in the context of a problem of plane stress. Drawing on the results with the stationary crack in which case this stress at the crack tip could be written as a product function of a time dependent stress intensity factor and a function representing this spatial distribution of the stresses, we write tentatively for the dynamic case

$$\sigma[\underline{x}(\underline{X},t),t] = K(t)f[\underline{x}(\underline{X},t);v] + a \qquad (41)$$

Although there exists an explicit form for the function $f(\underline{x};v)$ for the case of dynamically moving cracks in an elastic material this function is not available for the viscoelastic material. However, in order to arrive at an adequate estimate we note that the speed of cracks in viscoelastic materials tends to be relatively low. This observation allows us to disregard dynamic effects in this stress distribution so that we may make use of the quasi-static stress distribution as an approximation. In accordance with equation (34) we use

$$f(\underline{x}) = \left\{ \frac{x_1 + (x_1^2 + x_2^2)^{\frac{1}{2}}}{\pi\,(x_1^2 + x_2^2)} \right\}^{\frac{1}{2}} \qquad (42)$$

It is a general observation that for crack propagation velocities less than about half the Rayleigh surface wave speed, the error due to the use of quasi-static behavior is within the range of experimental error for the elastodynamic crack problem. Making use of this assumption, we obtain for the deflection vector of the light rays in passing through the deformed crack tip area, via equations (31), (34), (39) and (42) as

$$\underline{\omega}[\underline{x}(\underline{X},t)] = d_o z_o \text{grad}[\int_{-\infty}^{t} C(t-\xi)\{-K(\xi)v(\xi)\frac{\partial f}{\partial x_1}[\underline{x}(\underline{X},\xi)]$$

$$+ \frac{\partial K(\xi)}{\partial \xi} f[\underline{x}(\underline{X},\xi)]\} \, d\xi] \tag{43}$$

Upon integrating this by parts we obtain the result

$$\underline{\omega}[\underline{x}(\underline{X},t),t] = d_o z_o \{K(t)C(o)\text{grad } f[\underline{x}(\underline{X},t)] \tag{44}$$

$$+ \int_{t_o}^{t} C'(t-\xi)K(\xi)\text{grad } f[\underline{x}(\underline{X},\xi)]d\xi\}$$

where t_o denotes the time when the loading of $K(t)$ begins and $C'(t) = \frac{dC}{dt}$.

In order to compute the shape of the caustic we have to make use again of the condition that the Jacobian of the transformation

$$J = \frac{\partial(x_1',x_2')}{\partial(x_1,x_2)} = 0$$

represented by equations (30) and (45) vanishes. However, we are not really interested in the shape of the caustic for a given

history of the stress intensity factor. Rather, we are only
interested in the measurement of the stress intensity factor as a
function of velocity and time. It indeed turns out from experiments
described later that the shape of the caustic for a crack running
in a viscoelastic material is not much different at all from that
of the stationary crack for the velocities encountered in our
experiments. In order to determine the radius of the initial curve
it is therefore not necessary to compute the total shape of the
caustic; rather it is sufficient to compute this radius "r_o" by
using the condition that on the crack axis

$$\left|\frac{\partial x_1'}{\partial x_1}\right|_{x_2=0} = 0, \tag{45}$$

Let us make the further assumption that the stress intensity
factor varies slowly. This is actually a condition found in our
experiments. Then $\frac{\partial K}{\partial t} \approx 0$ and the second term in eq.
(43) is assumed to be negligibly small due to the structure of
the function $f[\underline{x}(\underline{X},\tau)]$. If in addition the acceleration of the
crack is small we can obtain from equation (43) the deflection
vector of the light rays as

$$\omega_1[\underline{x}(\underline{X},t),t] = -d_o z_o K(t) v(t) \int_{-\infty}^{t} C(t-\xi) \cdot \tag{46}$$

$$\cdot \frac{\partial^2 f}{\partial x_1^2}[\underline{x}(\underline{X},\xi)]d\xi$$

where

$$x_1(\underline{X}, \xi) = x_1(\underline{X}, t) + (t-\xi)v_o \tag{47}$$

and v_o denotes the speed of the crack. Then, the condition

$$\frac{\partial x_1'}{\partial x_1}\bigg|_{x_2=0} = 0 \ \left(\text{or } \frac{\partial w_1}{\partial x_1}\bigg|_{x_2=0} = -1\right)$$

renders the stress intensity factor

$$K = \frac{4\sqrt{2\pi}}{15 d_o z_o \int_o^\infty \dfrac{|C(x/v_o)|}{(r_o+x)^{\frac{7}{2}}} \, dx} \tag{48}$$

Let us now examine the limit expressions for the stress intensity factor in eq. (48) namely for the cases of vanishing and for infinite crack propagation velocity v_o. One has then

$$K = \frac{2\sqrt{2\pi}}{3 z_o d_o |C(\infty)|} \ r_o^{\frac{5}{2}} \qquad v_o \to 0 \tag{49}$$

$$K = \frac{2\sqrt{2\pi}}{3 z_o d_o |C(o)|} \ r_o^{\frac{5}{2}} \qquad v_o \to \infty$$

These expressions correspond to the elastic expressions except that the optical constants are replaced by $C(\infty)$ and $C(o)$, respectively. In general the function $C(\xi/v_o)$ is the function shown in figures 5 and 6 for Solithane 113 and Homalite 100, respectively.

In any experiment the diameter of the caustic along the line normal to the plane of crack propagation is used as a definition for the size of the caustic. This diameter D is

related to the radius of the initial curve by $r_o=mD$. For the
case of parallel incident light, this constant is, for a
stationary crack, equal to m = 1/3.17. We have now estimated the
size of the caustic and thus provided the tool to measure the
stress intensity factor instantaniously for a crack propagating
in a viscoelastic material.

7 APPEARANCE OF FRACTURE SURFACES SMOOTHNESS AND BRANCHING RELATED SURFACE FEATURES

In this section we discuss the physical appearance of
fracture surfaces generated in dynamic tests on Solithane-113
and Homalite-100. In either material the temperature was adjusted
so as to move towards the more viscoelastic response of the
material in the vicinity of the glass transition temperature. For
the polyester Homalite-100 which has a glass transition temperature
in the vicinity of 100°C this implied heating, while for the
polyurethene Solithane-113 with a glass transition temperature of
approximately -20°C this implied cooling.

Let us first consider the behavior of Homalite-100. An
initial set of tests was performed at distinct pressure levels and
different temperatures, namely, in a test matrix consisting of
pressures on the crack surfaces of 133, 357 and 805 psi. For each
of these pressure levels tests were conducted at 60, 80 and 100°C.
The objective was to determine whether the crack propagation rate
varies significantly as a function of temperature and/or how

branching was facilitated or suppressed. Figure 8 shows the appearance of the crack path in each one of these nine tests. One notes immediately that branching occurred only at 805 psi and this occurrence was not systematic with the temperature variation in the three tests, inasmuch as branching occurred at 60 and 100°C but not at 80°C. We only note in this context that the crack propagation rate for the 80°C and 805 psi test was slightly smaller than the velocity associated with the 60°C and 805 psi test.

The fracture surfaces corresponding to these tests are shown in figure 9 with a more detailed view of the 805 psi 60°C case shown in figure 10. Here we note that the appearance of the fracture surfaces reflects essentially the branching or non-branching characteristics of the test. Although this evidence may be difficult to identify in the reproductions of this figure in this report, closer examination of the actual photographs shows that the 133 psi tests all produced only smooth fracture surfaces. At 357 psi only the 60°C test produces a somewhat roughly textured surface while the 80 and 100°C tests produce smooth fracture surfaces. This appearance is in keeping with the somewhat smaller stress intensity factors encountered at 80 and 100°C when compared to the 60°C test. At 805 psi the 60°C test produces a typical transition in the appearance of the fracture surface from "smooth", to "mist", to "hackle", then branching [26]. At the same pressure at 80°C the surface remains relatively smooth, this

indicates that branching was not approached even closely. At
100°C and 805 psi most of the surface appears relatively smooth;
however, there is a short transition from mist to hackle which
indicates possibly that the branching in this particular test
was precipitated by a flaw in the specimen and, had it not been
for this flaw, no branching might have occurred. This statement
is, however, essentially conjectured. We are thus not able to
state definitively that increasing the viscous response of the
material will suppress branching, although the slight indication
in that direction exists but only further testing will allow us
to examine the possible truth of this statement.

We consider next the appearance of the fracture surfaces of
Solithane-113. The physical appearance of the failed specimen is
summarized in figure 11. First note that the path of crack
propagation is rather similar to that in Homalite 100. One
concludes from this that the mechanics of wave propagation and
the conditions that determine the instantaneous orientation of
crack propagation are apparently not markedly affected by the
viscoelasticity of the material response. Note also from the
temperatures indicated in that figure, that most of these
Solithane tests have been conducted at or below the glass
transition temperature. However, in none of the tests branching
has been observed.

When one studies the fracture surfaces they exhibit the
typical transition from smooth to rough as the stress intensity

factor increases and as branching is approached. It may appear
thus that branching was indeed approached but that the pressure
applied to the Solithane specimens was not quite large enough
to precipitate the branching phenomenon. The reason for this
failure to achieve branching in Solithane, may be two-fold. One
reason may be that the relatively large crack flank opening
displacements reduce the applied pressure and thus the stress
intensity. Moreover, the viscoelastic response can reduce the
stress intensity factor, also. However, as we have indicated earlier,
at temperatures of -20°C or below this reduction should be
relatively small because the material is essentially in its
glassy state. Hence we discount this reason for suppressing
branching. For the remaining reason we simply have to deal with the
fact that Solithane in its glassy state may be a considerably
tougher material than Homalite 100. If that is so, our failure to
achieve branching in Solithane 113 may simply due to the fact
that insufficently high pressures have been applied to date.

Let us now inquire into the mechanism of branching; the
basic question here is whether the phenomenon occurs in a
continuous growth process or whether branching is the result of
secondary fractures that link with the main crack. To date
evidence suggests that both occur.

One of the possible mechanisms is associated with crack path
instability: Suppose the crack path deviates slightly from the
original, straight path. We speak then of crack path stability if

the deviation increases, and stability if the path returns to the
original, straight one. For quasistatic problems crack path
instability is fostered by tension at the crack tip in the
direction of crack growth (first order term in the singularity
expansion) while stability is enhanced by a compressive stress.

We first observe that in the early stages of crack propagation
with our loading configuration, the crack path is stable. Figure
12 shows three photographs of fracture surfaces in which the
left hand side depicts the initial crack. Note that in each case
the initial crack does not fall on the same plane. The crack
face is composed of several different planes which have different
levels and directions. In each case these different crack planes
coalesce into one main crack. We deal here thus clearly with
crack path stability.

This stability may be explained in terms of energy expenditure.
Clearly the crack wants to propagate at the maximal rate with a
minimum of energy expenditure. The growth of the crack on
different planes obviously requires more energy than for growth
in one plane, because the total area generated is larger than
for one planar crack if the local crack speeds are equal. Thus
one deduced that for low intensity cracks, when just enough energy
is available to drive the crack, that path is stable.

We insert here a side remark concerning figure 12 that
relates to the surface roughness. The top figure results from a

test at 60°C and 357 psi pressure: The fracture surface is glass-like and smooth. However, in the other two photographs, resulting from tests at 805 psi and 80°C and 100°C, respectively, one notices increased roughness with temperature increase, which roughness, however disappears. The conclusion is thus close at hand that this feature is associated with the transient generation of the plastic zone established as part of the initial loading process.

We return now to the question of crack path stability and consider the behavior of the crack at branching. Figure 13 shows views of surfaces that are mating up to the line of branching. While it is difficult to reproduce the pertinent features of these fracture surfaces, a direct visual inspection which renders the true three dimensional geometry reveals the following: In the upper photograph the upper edge exposes a continuous surface across the branch "line"; this represents a smooth turning of the crack near the specimen surface away from the main crack and into the paper (i.e. away from the viewer). The same feature is observed in the upper right hand corner of the lower photograph, which is near the specimen surface opposite from that referred to in connection with the upper photograph. Thus, on one side of the specimen a crack grows away from the main crack in, say, the "up"-direction while at the opposing specimen surface, the surface near crack is in the "down" direction. Thus branching would occur in an assymmetric fashion from the surface of the specimen, with subsequent crack growth sidewards towards the middle. Evidence of

this "side-cutting" is visible in the upper photograph of figure
13 where striations at right angles to the direction of general
crack growth indicate that locally and temporarily crack
progression occurred transversely to the plate. This mechanism may
be helpful for the interpretation of continuous surface generation
and energy release rate before and after branching [27]. We note
that we are aware, that this potential mechanism of branching is
tied to the finite thickness of the test geometry, and unduely so.
For this reason we are now examining also discontinuous mechanisms
in which secondary fractures away from the main crack become
responsible to open new paths for crack propagation.

8 DYNAMIC CRACK PROPAGATION BEHAVIOR - CRACK SPEED
DEPENDENCE ON LOADING AND TEMPERATURE

In the previous section we have indicated the test matrices
on temperature and (nominal) applied pressure for Homalite 100 and
for Solithane 113. In this section we discuss the crack propagation
response resulting from these investigations. Let us consider the
Homalite tests first. A typical high speed photograph of caustics
(60°C, 805 psi) is shown in Fig. 14(a) and (b) for the measurement
of the history of the stress intensity factor. The stress intensity
histories for the test matrix are shown in figure 14(c). We note
that even after the cracks have started to run there is a significant
variation in the magnitude of the stress intensity factor, however,
there are no sudden changes in these traces, so that, on first
inspection, the assumption made in the analytic section, namely
that $\partial K/\partial \tau = 0$, is not unreasonable. It turns out, that inspite of

the readily measurable variation in the stress intensity factor the velocity of crack propagation is constant within the accuracy of our measurements. These results are plotted in figure 15 where one notes a clear trend to lower velocities with increasing temperature. Note also that there exists a minor decrease in the stress intensity factor with increasing temperature - also clear from figure 16 - which arises from the material softening and the effect which this softening has on the stresses transmitted from the copper loading strips to the specimen. This latter phenomenon will be considered in more detail later on.

In figure 17 we compare these tests at elevated temperatures to room temperature tests performed by other investigators [28]. Again one observes the clear temperature related trend to lower crack speeds for comparable stress intensity factors. This observation is documented graphically more clearly in figure 16.

For Solithane 113 we show the time traces for the stress intensity factor in figure 18. Note that the initial portions of these traces are estimated and thus shown dotted. The uncertainty arises from the following fact: The pressure producing copper conductor in the crack generates a steady state pressure on the crack surfaces which, in turn, generates a caustic at the bend of the copper strip. This bend is close to the crack tip: the caustic associated with this bend remains stationary as the crack grows.

Because the caustic induced by the copper strip is large the smaller caustic resulting from the crack tip stresses is first engulfed in the former and some time of crack growth has to pass

before the dynamically induced caustic emerges from the dark
field of the initial stationary caustic.

The sequence shown in figure 18 indicates the response of
crack growth in tests conducted at different temperatures. As
discussed in section 7 there are (probably) two causes for the
change in crack speed, one being the change of material compliance
with temperature, the other the effect of energy dissipation
associated with different temperatures. At this time these two
effects cannot be separated clearly; a more complete test matrix
is required. In addition, our newly developed capability of
evaluating caustics for cracks running in viscoelastic solids
allow us now to attempt the construction of this test matrix in
terms of stress intensity factor and temperature instead of the
nominal pressure applied to the crack faces. For now we merely
plot in figure 19 the velocity of crack growth as a function of
temperature, being well aware that this dependence is at least
in part due to the change in stress intensity, (also indicated in
figure 18).

9 ESTIMATION OF LOAD VARIATION RESULTING FROM TEMPERATURE INDUCED CHANGES IN MATERIAL STIFFNESS

Recall that the pressure is applied to the crack surfaces
via a double bent copper strip in which a mechanical force is
generated by virtue of a flowing current and the induced magnetic
field (cf. figure 20). The pressure depends on the separation of

the two conductors. If the separation is small, the pressure is high; if the separation is large the converse is true. Thus if a relatively rigid material is used in the experiments the separation of the conductors will remain small for the duration of the test. However, if the material is relatively compliant then the induced force will separate the crack surfaces during the later phase of the pressure pulse, carrying the conductor with it and allow wider separation. Therefore during the latter portions of the experiments the driving force will drop off. This phenomenon may be responsible for generally reducing the stresses at the crack tip so that they are lower than we might have otherwise expected. It is the purpose of the immediate following developments to estimate the amount of pressure loss due to this effect. This pressure loss is then translated into an estimate of the stress intensity factor history if the crack tip were to remain stationary. This procedure will provide us with a rough estimate, therefore, of a more realistic stress intensity factor history even at a tip of a moving crack indicating primarily substantial loss over which one might expect from a high modulus test material.

In addition to the pressure reduction due to the relatively low rigidity of one of the test materials one finds that the viscoelastic response has an effect on this stress intensity factor history. The magnitude of this effect, which turns out to be also a reduction in the stress intensity factor, is estimated

by drawing on the computation for the stress intensity factor from the anti-plane problem discussed in section 3.

We start with considering the effect of material rigidity without specific viscoelastic response. The ingredient of this estimation is first a knowledge of the instantaneous force supplied by the conductor strips to the crack faces as a function of this separation. The analytical treatment of this has been given in a previous report [29] and is reproduced here in figure 21. If one knew therefore what the instantaneous separation of the strips is one could deduce the pressure pulse history to the crack surface. Accordingly the strip separation has been determined photographically in an experiment. The result of this is shown in figure 22 and the time dependent evaluation in figure 23. Using figures 21 and 23 one computes therefore the instantaneous pressure applied to the crack surfaces as given in figure 24.

Note that for the compliant Solithane material which corresponded to the properties at $20^{\circ}C$ there is a considerable loss of pressure at times roughly beyond 50-60 μs. The present arrangement therefore produces a load history that is more appropriately represented by a pressure pulse on the order of 60 μs roughly with a ramp type loading and ramp type unloading. Drawing again for a moment on purely elastic results which have been calculated elsewhere [30] and as shown in the left inset in figure 25, we can, by a superposition of that result in terms of loading and delayed unloading of the same type, compute the stress

intensity factor for a pressure pulse as indicated in the right inset in that figure. Thus while a relatively stiff material such as Homalite 100 at room temperature would produce significant stress intensities for times on the order of a 100 to 150 μs the softer Solithane type of material at least for temperatures around room conditions would produce stress intensities that are approximately 25% of that produced in Homalite 100, although at short times up to approximately 50 μs the same kind of stress intensities would probably result.

Let us now turn to estimate the effect of <u>viscoelastic</u> behavior on this stress intensity factor. In order to do this we draw on the results in the earlier section 3 in which this stress intensity factor for the anti-plane shear mode in a viscoelastic material was considered. Because we lack any type of viscoelastic stress analyses for the opening mode - i.e. for the inplane deformation mode of the crack - we make use of the antiplane shear mode for an estimation of the amount by which the elastic stress intensity factor might be reduced as a result of viscoelastic material properties.

Recall that the Laplace transform of this stress intensity factor was given as equation (25);

$$\bar{K} = \sqrt{\frac{2\sqrt{\bar{\mu}}}{\sqrt{\rho s}}} \; \frac{\tau_o}{s} \tag{25}$$

note also that in the event of purely elastic properties in which
the shear modulus is given by the glassy shear modulus

$$\bar{\mu} = \mu_o/s \tag{50}$$

The transform of the glassy elastic intensity would be given by

$$\bar{K}_{g.e.} = \frac{2}{s} \frac{\mu_o}{\rho} \frac{\tau_o}{s} \tag{51}$$

deviding equation 50 by 52 results in

$$\frac{\bar{K}}{\bar{K}_{g.e.}} = \{\frac{s\bar{\mu}}{\mu_o}\} \tag{52}$$

The Laplace inverse of this equation poses in general some
difficulty and must therefore be accomplished by numerical means.
However, we believe that for our present estimation purposes it is
sufficient to accomplish this inversion in terms what is known
as a quasi elastic solution and write therefore that the stress
intensity factor is given as

$$K(t) = K_{g.e.} \{\frac{\mu(t)}{\mu_o}\}^{\frac{1}{2}} \tag{53}$$

The function in curly brackets is shown in figure 26 at 0^oC. The
time dependent stress intensity factor as given by equation (53)
is then shown in figure 27; for purely elastic response the ratio
of $\mu(t)/\mu_o$ equals unity. Thus the curve indentified as the
elastic one corresponds to the glassy response of the material. It

is clear that Solithane 113 at 0°C produces approximately only
half the stress intensity factor that one would expect from the
material if it were to undergo only small deformations and respond
with its glassy properties. This statement is more thoroughly
amplified by showing also the effect of lowering the temperature
in that at a temperature of -20°C this stress intensity factor is
only marginally smaller than the one represented for purely
elastic properties. Recall now that fracture tests were conducted
at temperatures of -20°C and lower. Hence for those tests it does
not appear that viscoelasticity is a significant detriment to
the generation of the stress intensity.

REFERENCES

1. P. Manogg, _Anwendung der Schattenoptik zur Untersuchung des Zerreissvorganges von Platten_, Ph.D. dissertation, University of Freiburg (1964).

2. P.S. Theocaris and E.E. Goloutos, "An Optical Method for Determining Opening-Mode and Edge Sliding-Mode Stress Intensity Factors", Journal of Applied Mechanics, 39, pp. 91-97 (1972).

3. J. Beinert and J.F. Kalthoff, "Experimental Determination of Dynamic Stress Intensity Factors by the Method of Shadow Patterns", Chapter in _Mechanics of Fracture_, VII. (edited by G.C. Sih), to appear in 1981.

4. A.J. Rosakis,"Analysis of the Optical Method of Caustics for Dynamic Crack Propagation", _Engineering Fracture Mechanics_, 13, pp. 331-347 (1980).

5. A.J. Rosakis and L.B. Freund, "The Effect of Crack-Tip Plasticity on the Determination of Dynamic Stress-Intensity Factors by the Optical Method of Caustics", _Journal of Applied Mechanics_, 48, pp. 302-308, (1981).

6. G.C. Smith and W.G. Knauss, "Experiments on Critical Stress Intensity Factors Resulting from Stress Wave Loading", _Mech. Res. Comm._, Vol. 2, No.4, pp. 187-192, Pergamon Press (1975).

7. B.R. Baker, "Dynamic Stress Created by a Moving Crack", _Journal of Applied Mechanics_, pp. 449-458, (1962).

8. B.V. Kostrov, "On the Crack Propagation with Variable Velocity", _International Journal of Fracture_, 11, No.1, pp. 47-55 (1975).

9. J.D. Achenbach and L.M. Brock, "Rapid Extension of a Crack", _Journal of Elasticity_, 1, pp. 51-63, (1971).

10. F. Erdogan, "Crack Propagation Theories", _Fracture_, 2, Chap. 5., pp. 497-590, H. Liebowitz (ed.), Academic Press, N.Y. (1968).

11. L.B. Freund, "The Stress Intensity Factor Due to Normal Impact Loading of the Faces of a Crack", <u>International Journal of Engineering Science</u>, 12, pp. 179-189 (1974).

12. L.B. Freund, "Crack Propagation in an Elastic Solid Subjected to General Loading - I. Constant Rate of Loading", <u>Journal of the Mechanics and Physics of Solids</u>, 20, pp. 129-140 (1972).

13. L.B. Freund, "Crack Propagation in an Elastic Solid Subjected to General Loading - II. Non-Uniform Rate of Extension", <u>Journal of the Mechanics and Physics of Solids</u>, 20, pp. 141-152 (1972).

14. L.B. Freund, "Crack Propagation in an Elastic Solid Subjected to General Loading - III. Stress Wave Loading", Journal of the Mechanics and Physics of Solids, 21, pp. 47,61, (1973).

15. L.B. Freund, "The Analysis of Elastodynamic Crack Tip Stress Fields", <u>Mechanics Today</u>, III, pp. 55-91, (1976).

16. J.D. Achenbach, "Dynamic Effects in Brittle Fracture", <u>Mechanics Today</u>, I, Chap. I, pp. 1-52, Nemat-Nasser (ed.), Pergamon, N.Y. (1974).

17. C. Atkinson and R.D. List, "A Moving Crack Problem in a Viscoelastic Solid", <u>International Journal of Engineering Science</u>, 10, pp. 309-322 (1972).

18. C. Atkinson and C.H. Popelar, "Antiplane Dynamic Crack Propagation in a Viscoelastic Strip", <u>Journal of the Mechanics and Physics of Solids</u>, 27, pp. 431-439, (1979).

19. J.D. Achenbach and C.C. Chao, "A Three-Parameter Viscoelastic Model Particularly Suited for Dynamic Problems", <u>Journal of the Mechanics and Physics of Solids</u>, 10, pp. 245-252 (1962).

20. A.T. deHoop, "Representation Theorems for the Displacement in an Elastic Solid and Their Application to Elastodynamic Diffraction Theory", Doctoral Dissertation, Technische Hogeschool, Delft (1958).

21. M.L. Williams, "On the Stress Distribution at the Base of a Stationary Crack", Journal of Applied Mechanics, 24, pp. 109-114, (1959).

22. G.R. Irwin, "Analysis of Stresses and Strains Near the End of a Crack Traversing a Plate", Journal of Applied Mechanics, 24, pp. 361-364, (1959).

23. M.L. Williams, W.M. Beebe, R.J. Arenz and C.W. Ferguson, "The Mechanical and Optical Characterization of Solithane 113 and Investigation of Optical Lag in Photoviscoelastic Analysis", GALCIT SM 64-42, WL TR-64-155, California Institute of Technology (1964).

24. W. M. Beebe, "An Experimental Investigation of Dynamic Crack Propagation in Plastic and Metals", Ph.D. Thesis, California Institute of Technology, (1966).

25. W.G. Knauss, "On the Steady Propagation of a Crack in a Visco-elastic Sheet: Experiments and Analysis" Deformation and Fracture of High Polymers, pp. 501-541, Edited by H. Henning Kausch et al., Plenum Press (1973).

26. A.S. Kobayashi, B.G. Wade, W.B. Bradley and S.T. Chiu, "Crack Branching in Homalite-100 Sheets", Engineering Fracture Mechanics, 6, pp. 81-92 (1974).

27. J.D. Eshelby, "The Elastic Field of a Crack Extending Non-uniformly Under General Anti-Plane Loading", Journal of the Mechanics and Physics of Solids, 20, pp. 129-140, (1972).

28. J.W. Dally, "Dynamic Photoelastic Studies of Fracture", Experimental Mechanics, 19, pp. 349-361, (1979).

29. M.C. Gupta and W.G. Knauss, <u>Dynamic Fracture in Viscoelastic Solids</u>, First Annual Report of Navy Contract # N00014-78-C-0634, California Institute of Technology, (1979).

30. G.C. Smith; "An Experimental Investigation of the Dynamic Fracture of a Brittle Material" Ph.D. Thesis, California Institute of Technology, Pasadena, California, 1975.
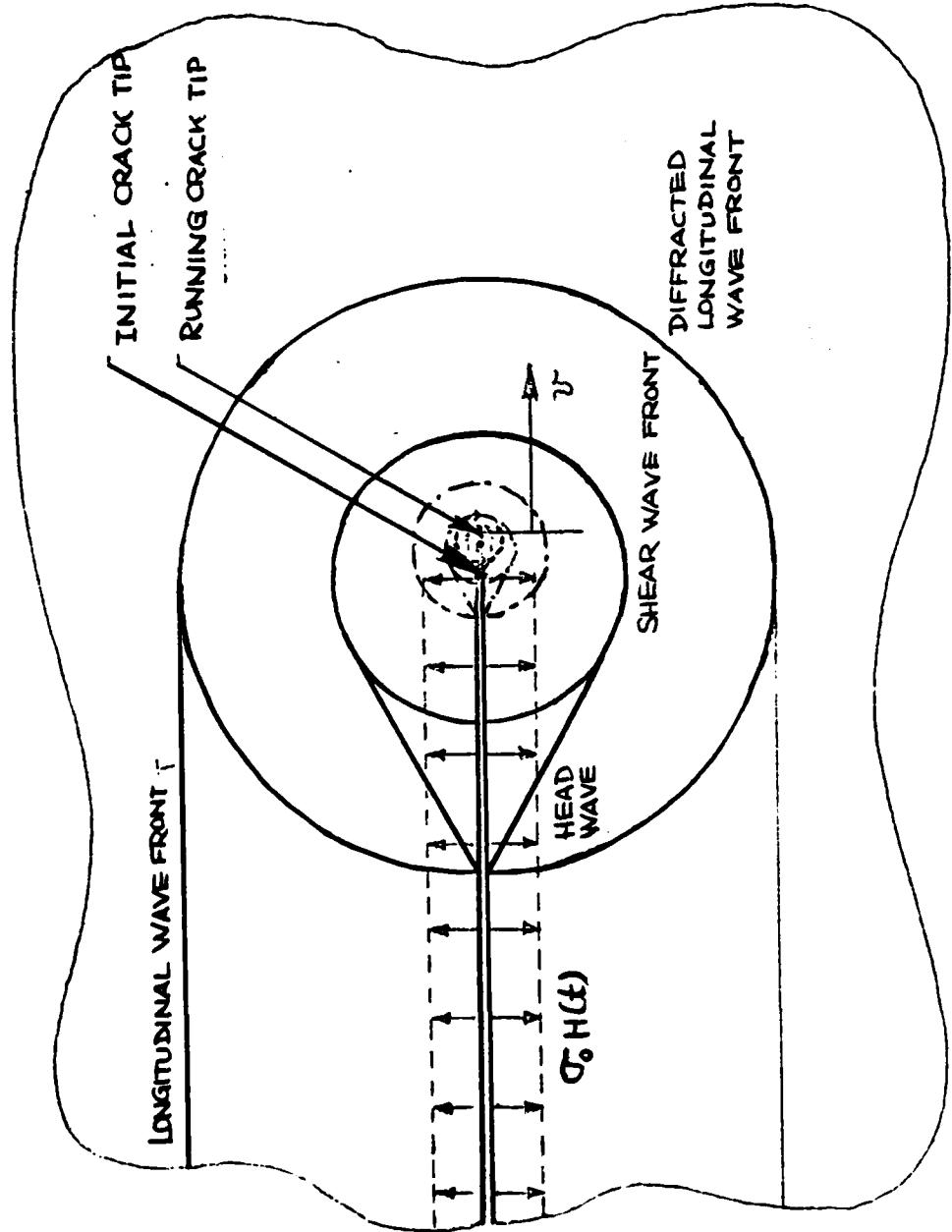
Fig.1 Schematic of Dynamic Loading on Semi-Infinite Crack
Faces
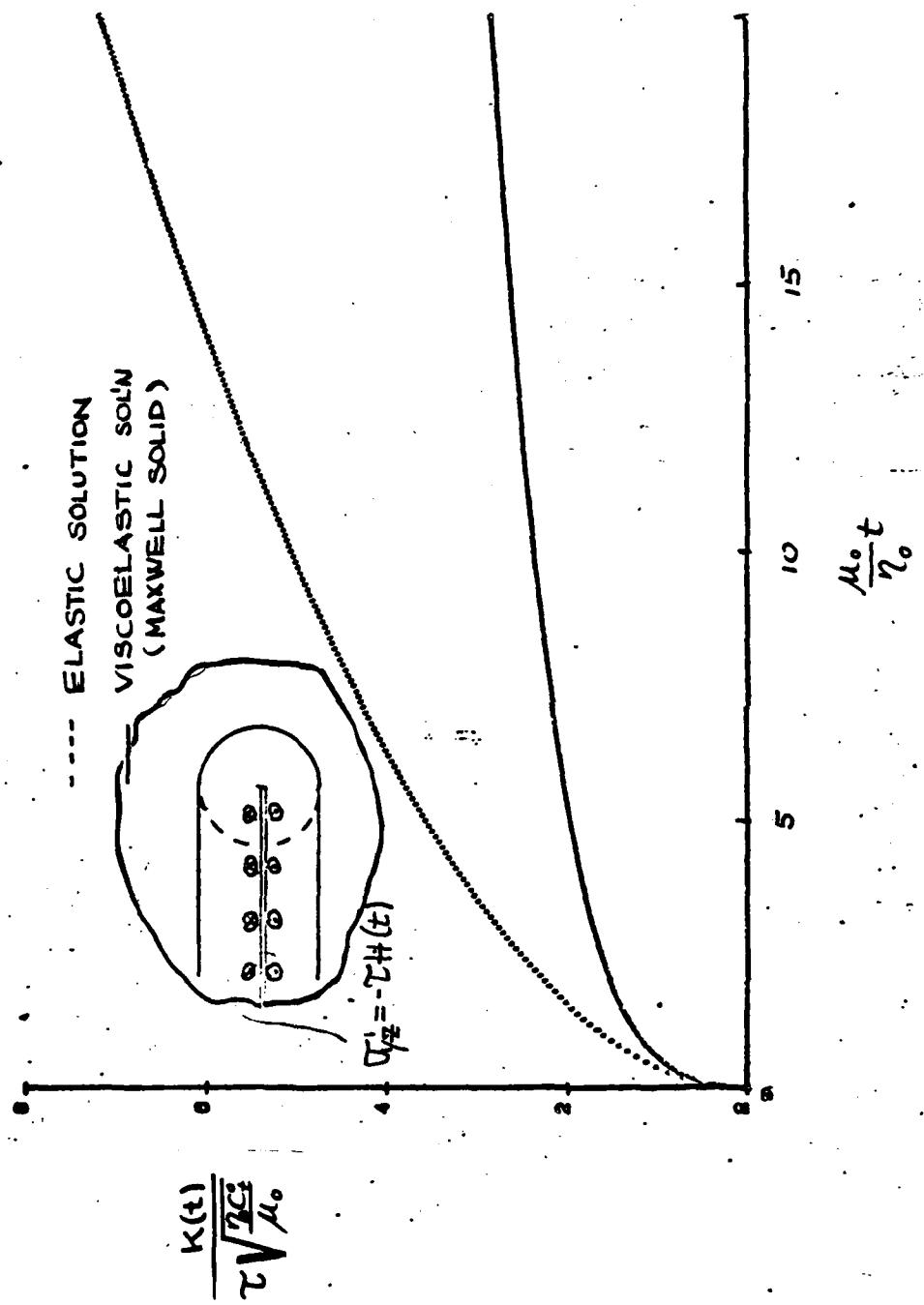
Fig. 2(a) Stress Intensity Factor Resulting from Dynamic
Loading (Mode III, Stationary Crack)

ELASTIC SOL'N

VISCOELASTIC SOL'N
(MAXWELL SOLID)

$$\frac{K(t)}{\tau\sqrt{\frac{2c_i}{\mu_o}}}$$

$$\frac{\mu_o}{\eta}t$$
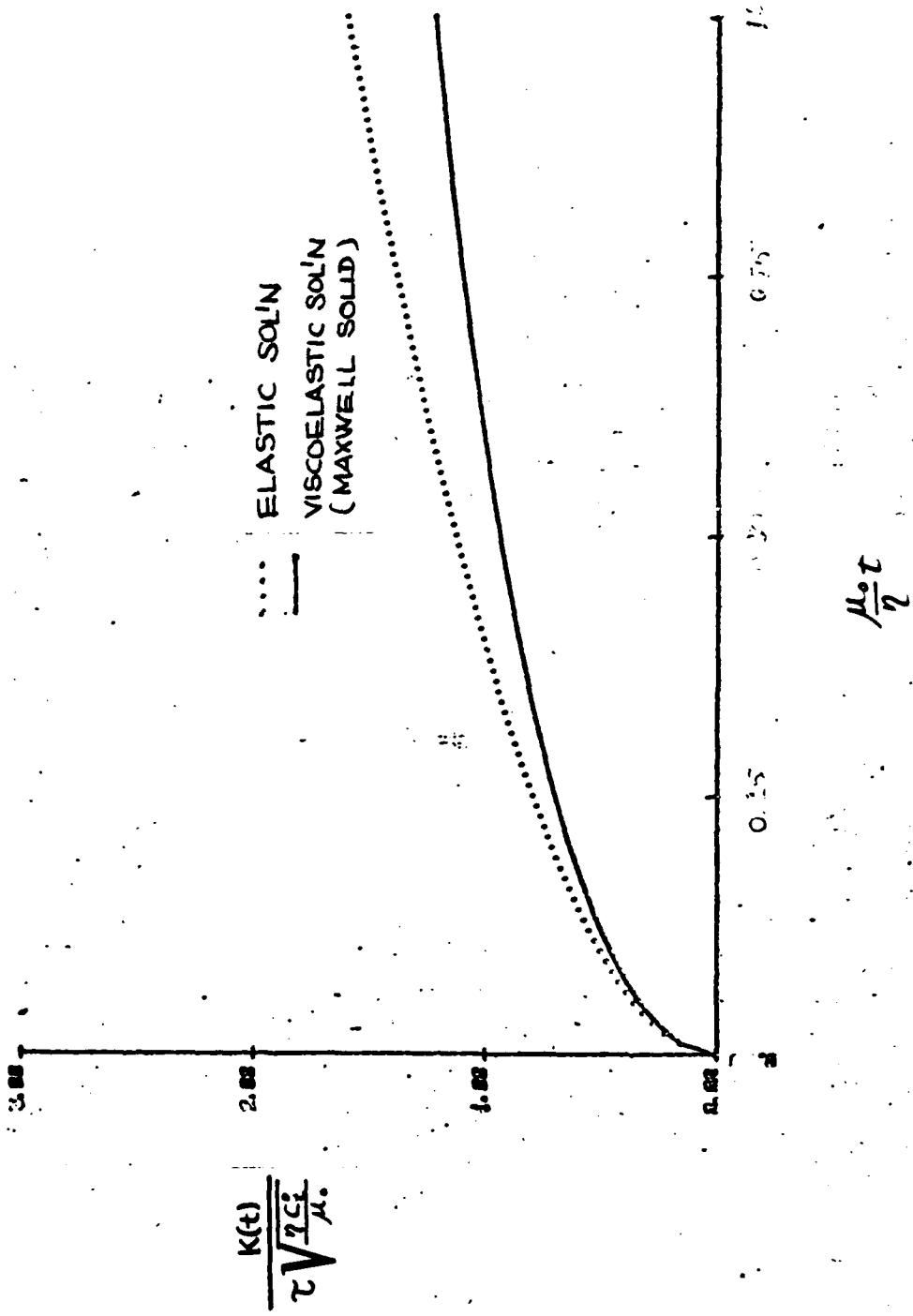
Fig. 2(b) Stress Intensity Factor Resulting from Dynamic
Loading (Mode III, Stationary Crack; Short Time
Behavior)
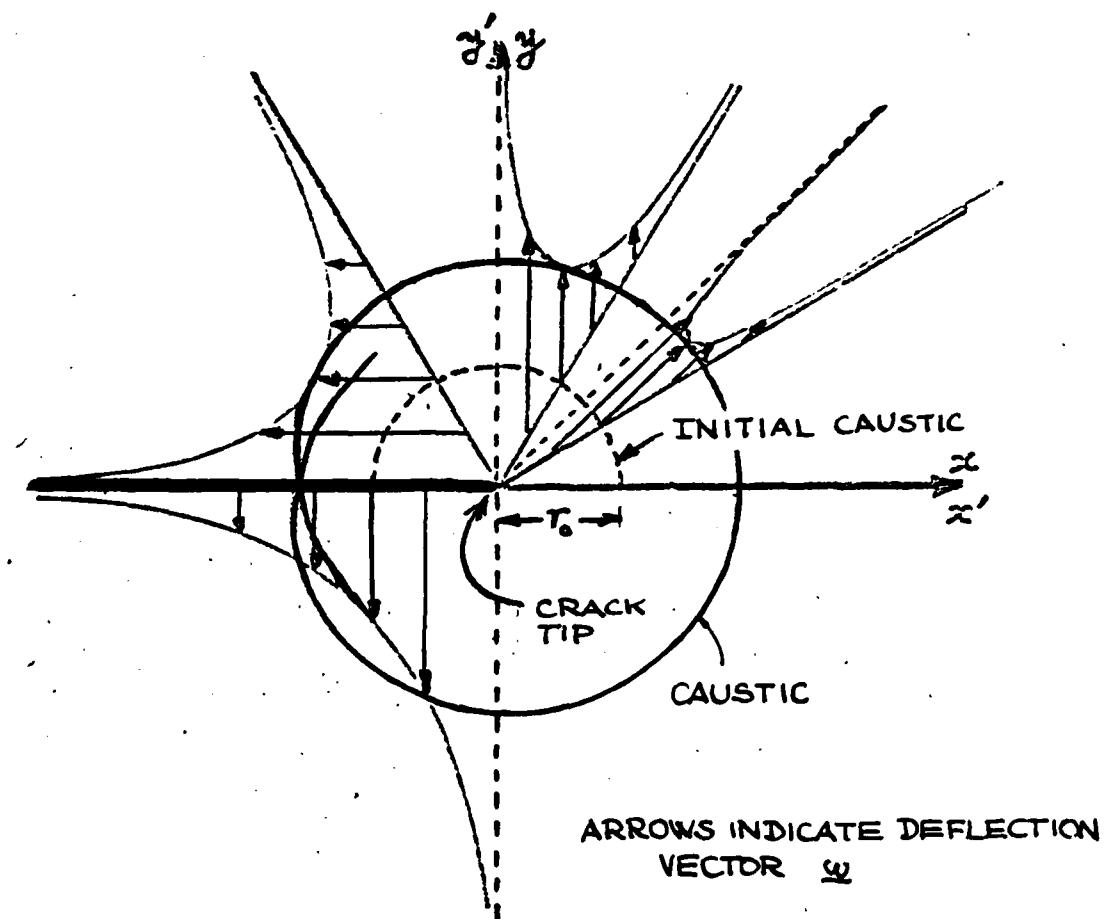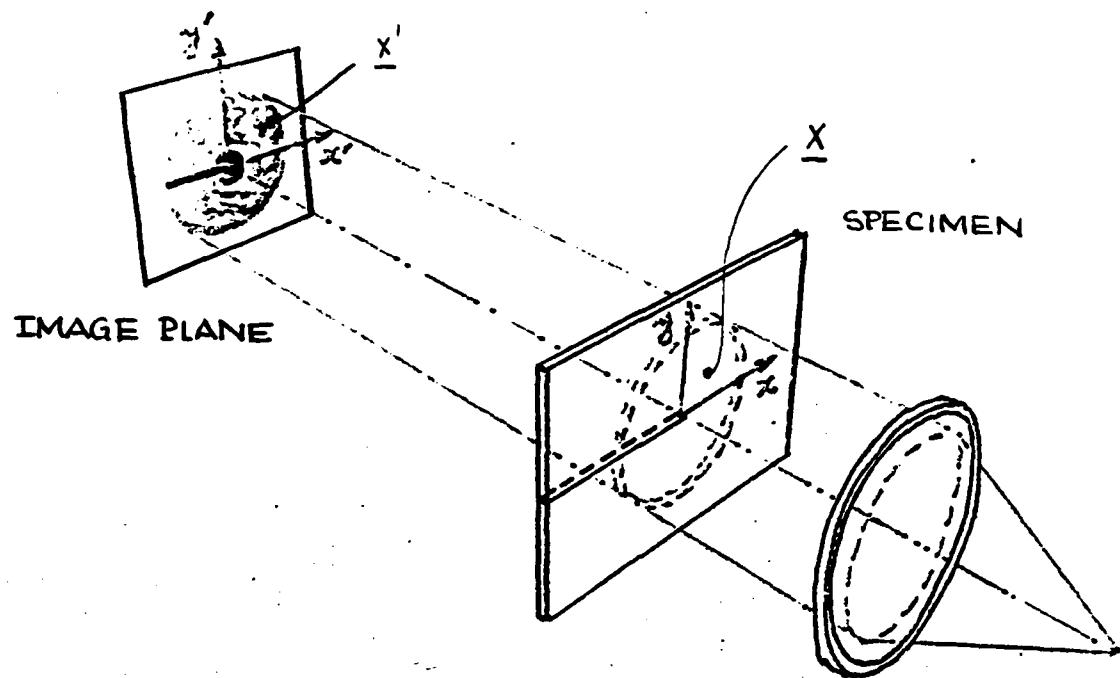
Fig. 3 Optical Method of Caustics

-10°C

before loading | 6sec | 12 sec | 24 sec | 1 min

1.5 min | 2 min | 3 min | 5 min | 7.5 min

10 min | 15 min | 20 min | 27 min
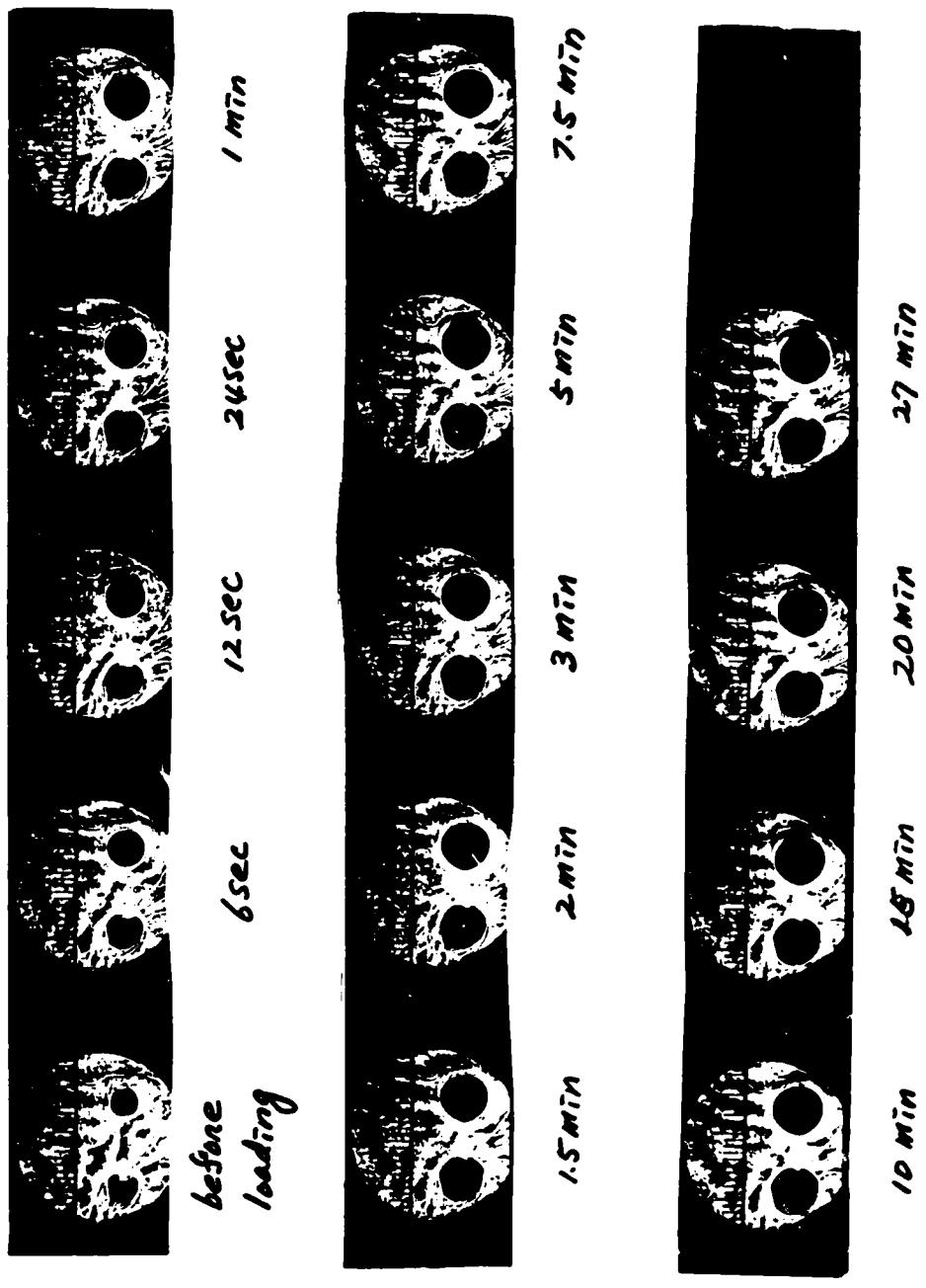
Fig. 4(a) Caustic Growth in Solithane 113 at -10°C
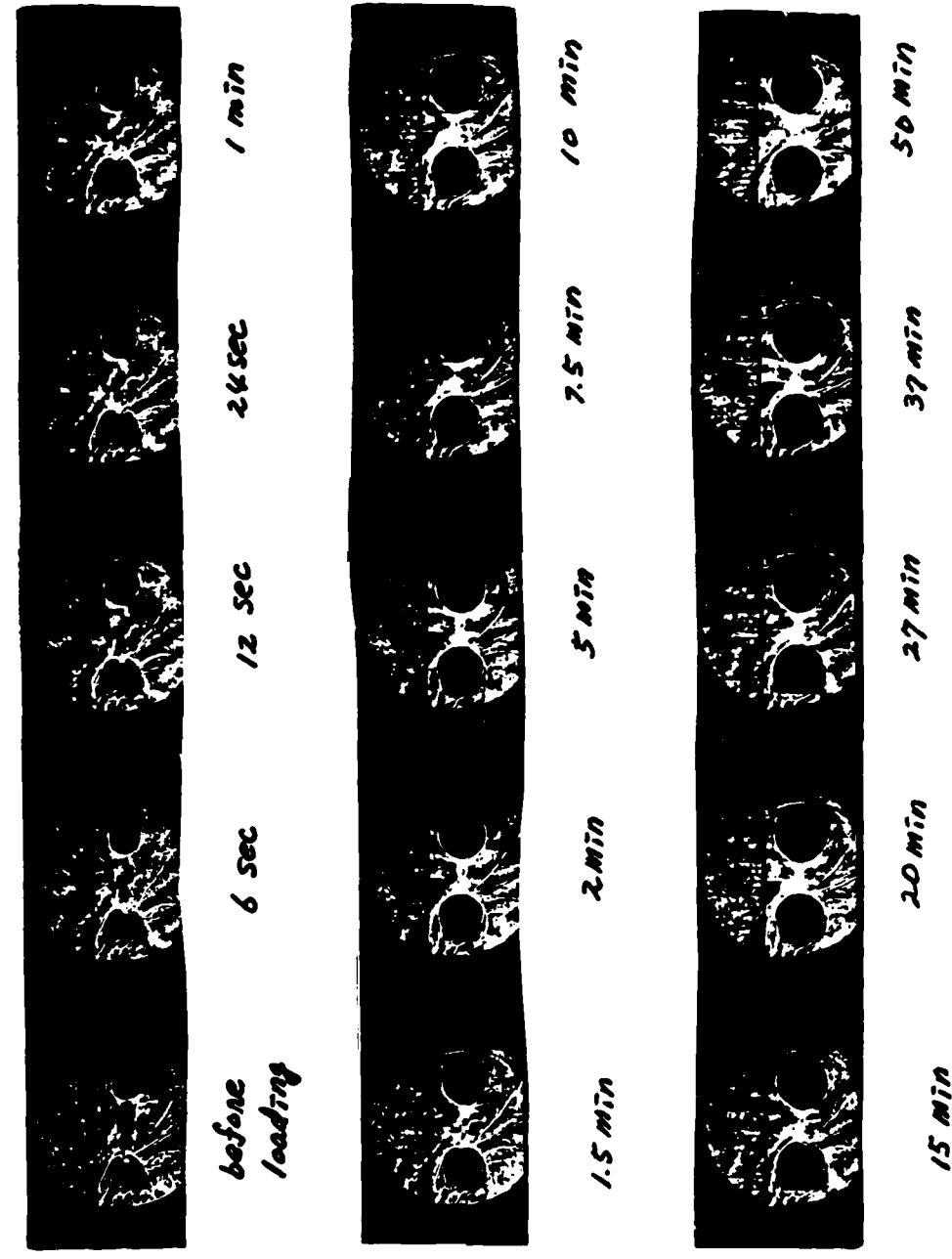
Fig. 4(b) Caustic Growth in Solithane 113 at -15°C
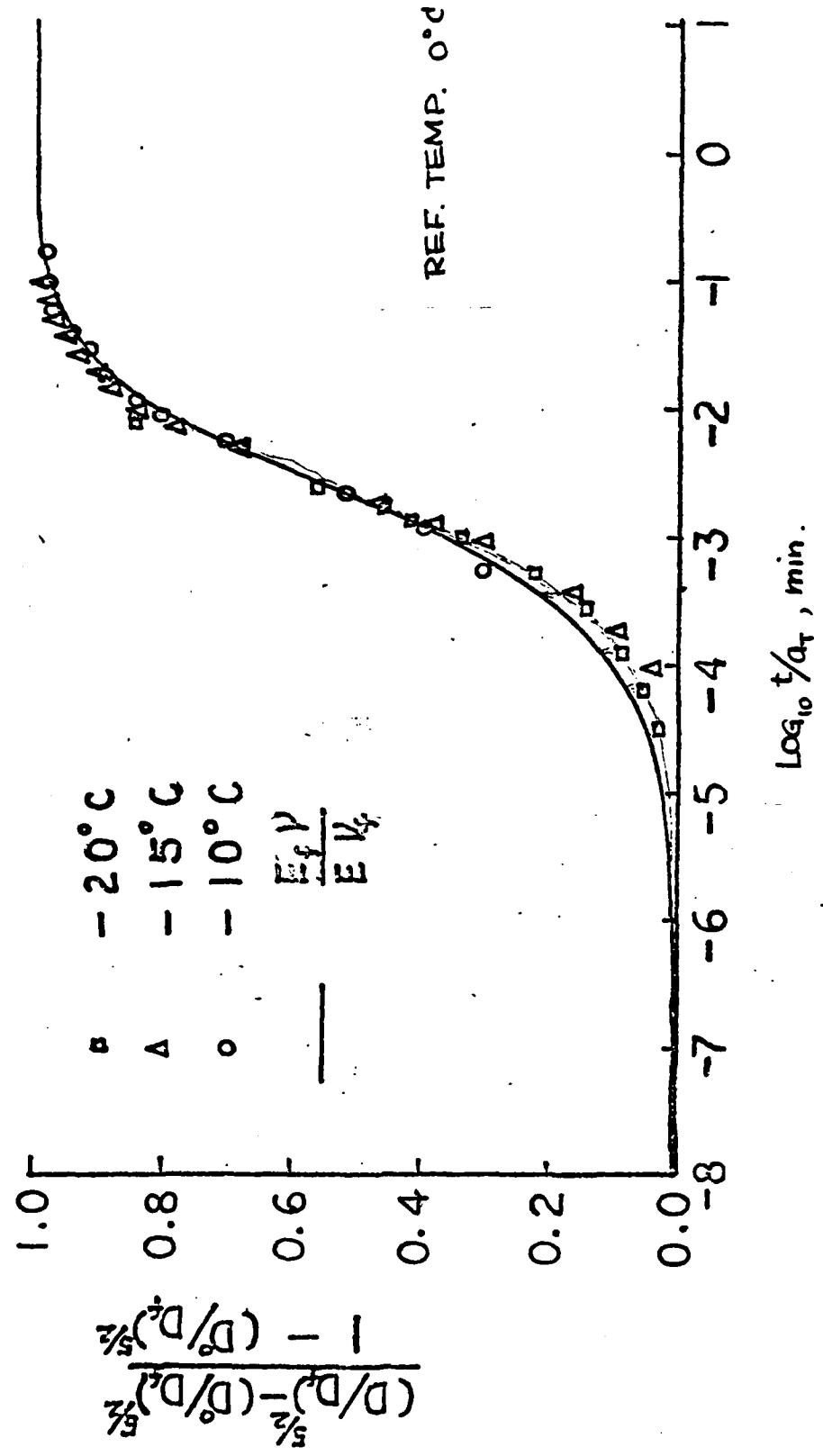
Fig. 5   Caustic Growth Curve for Solithane 113
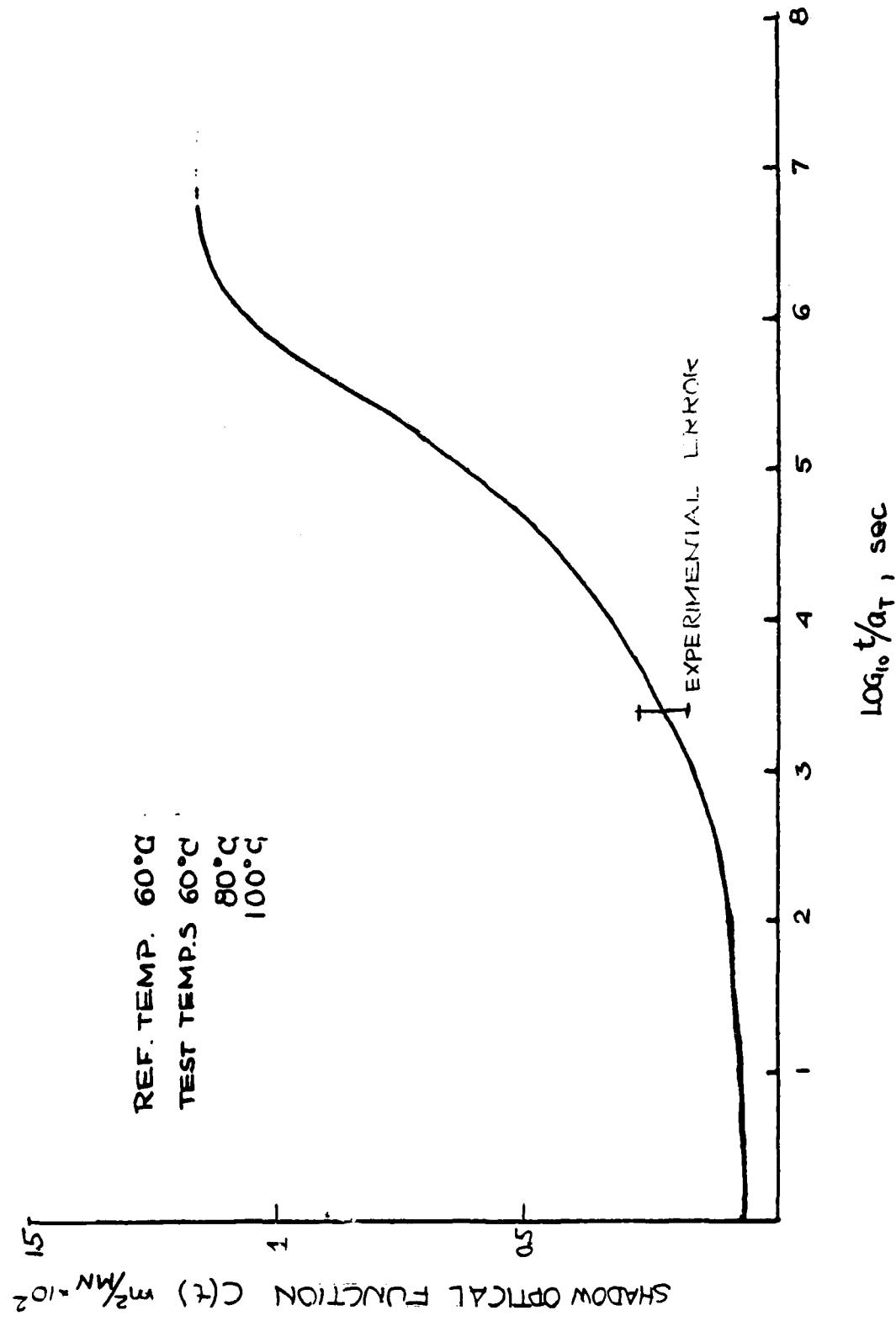
Fig. 6 Shadow Optical Function C(t) for Homalite 100
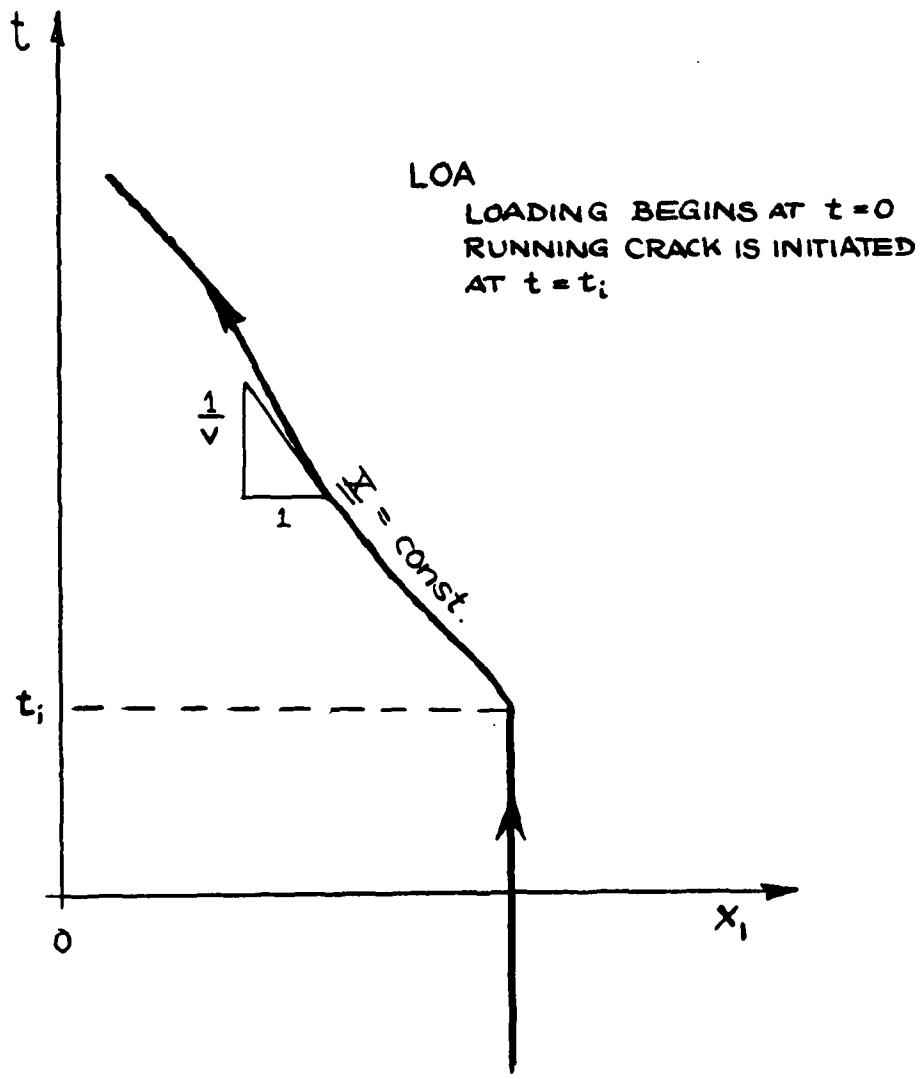
Fig. 7 Typical Trajectory of $\underline{x}(\underline{X}, t)$ for a Fixed Point of $\underline{X}$
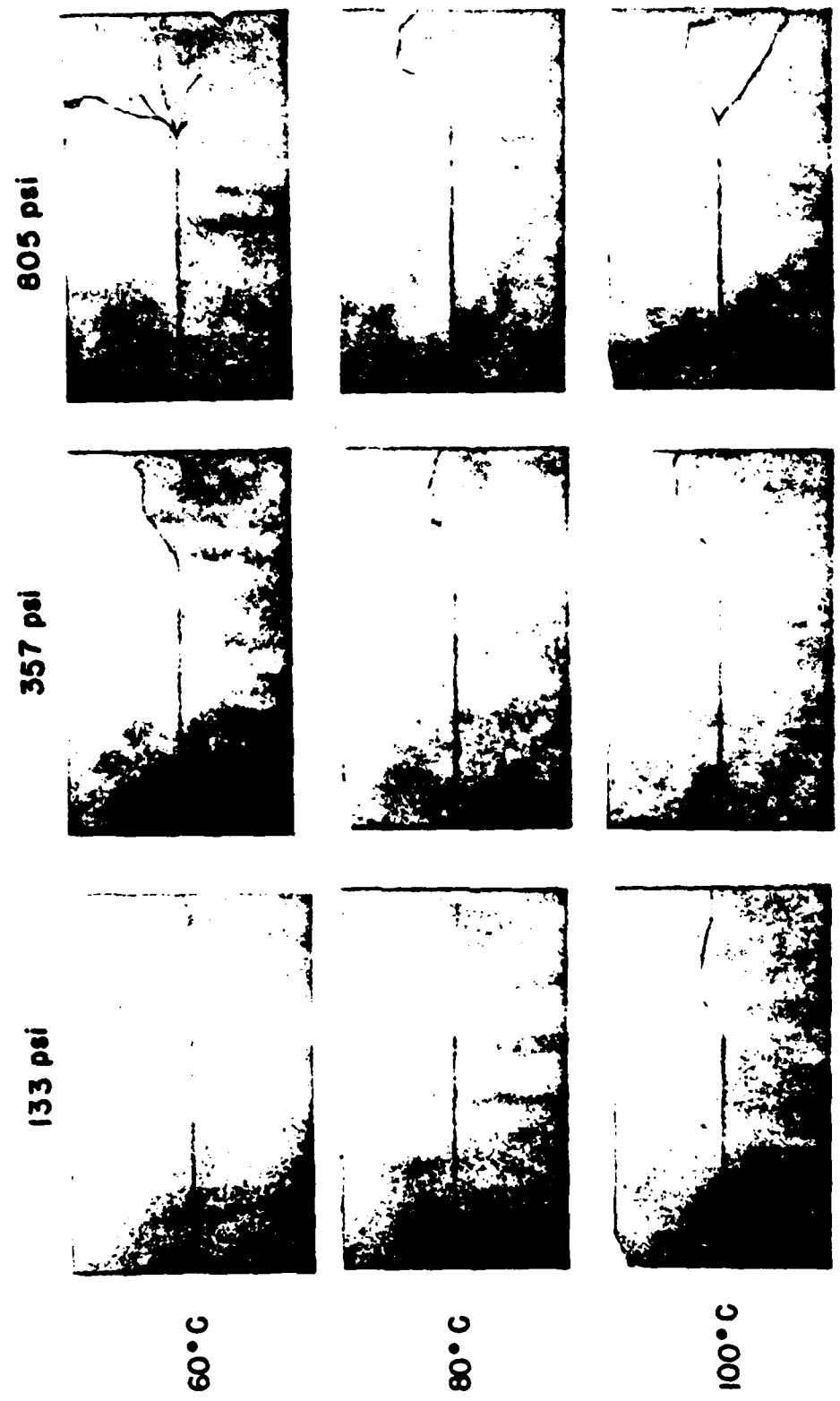
Fig. 8 Fracture Paths in Homalite 100
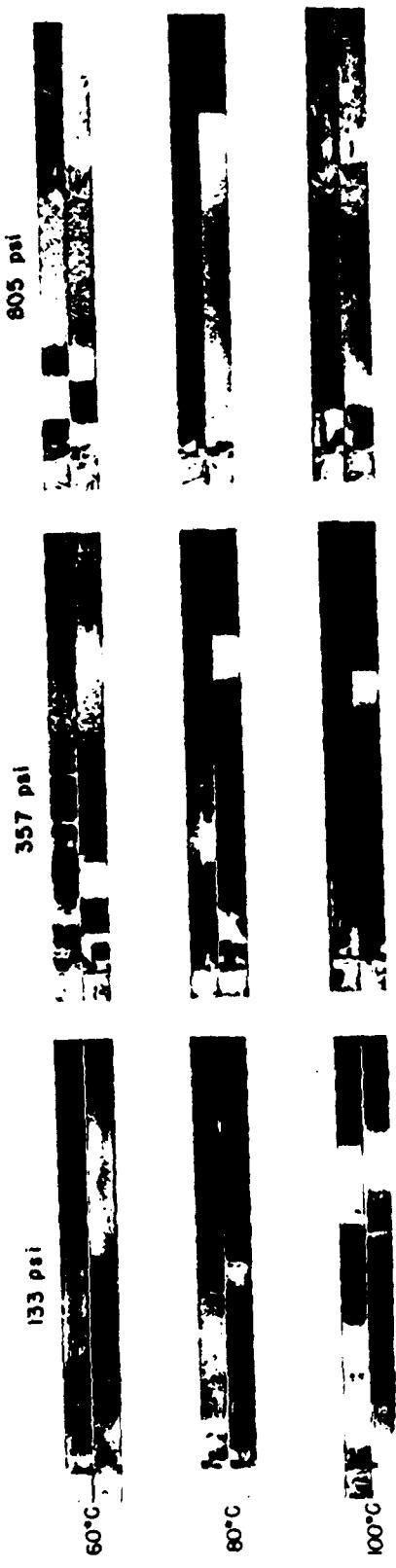
Fig. 9 Fracture Surfaces in Homalite 100
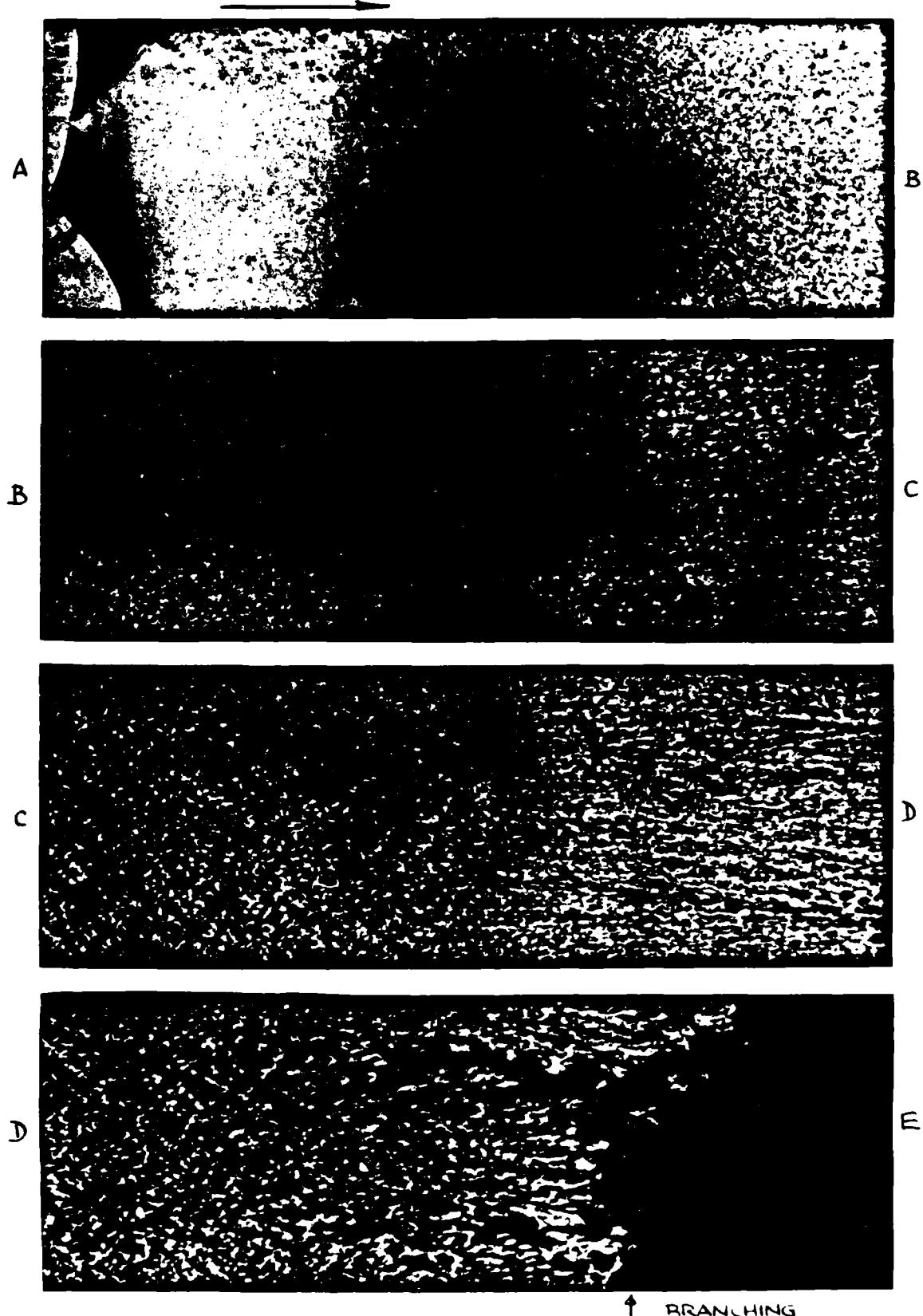
Fig. 10 Fracture Surface Detail of Homalite 100 Test at
305 psi and 60°C

-20°C   10 KV
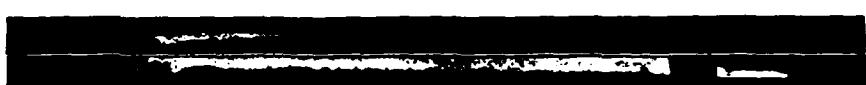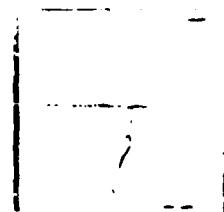
-40°C   10 KV
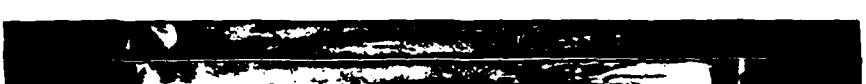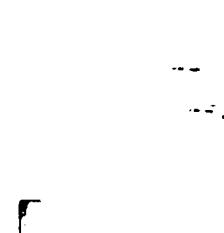
-40°C   12 KV
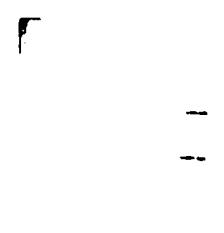
-40°C   14 KV
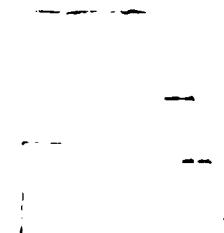
-60°C   10 KV
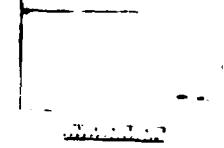
Fig. 11   Fracture Surfaces in Solithane 113

a) 60°C ; 357 psi
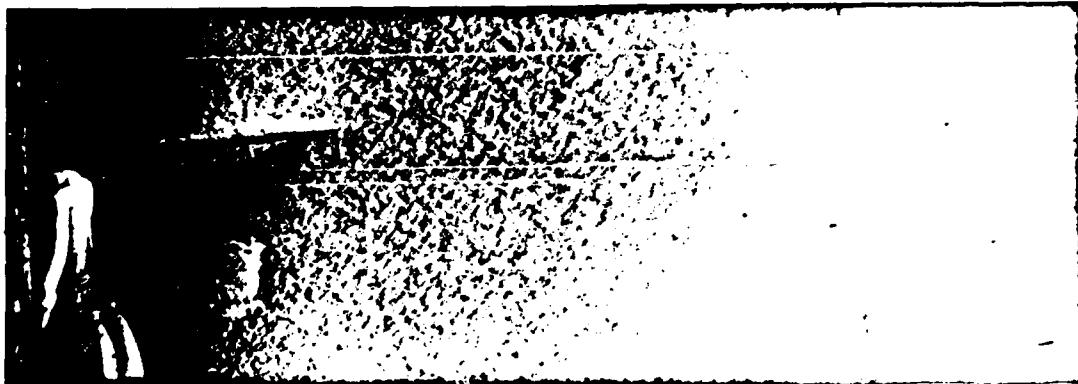
b) 80°C ; 805 psi
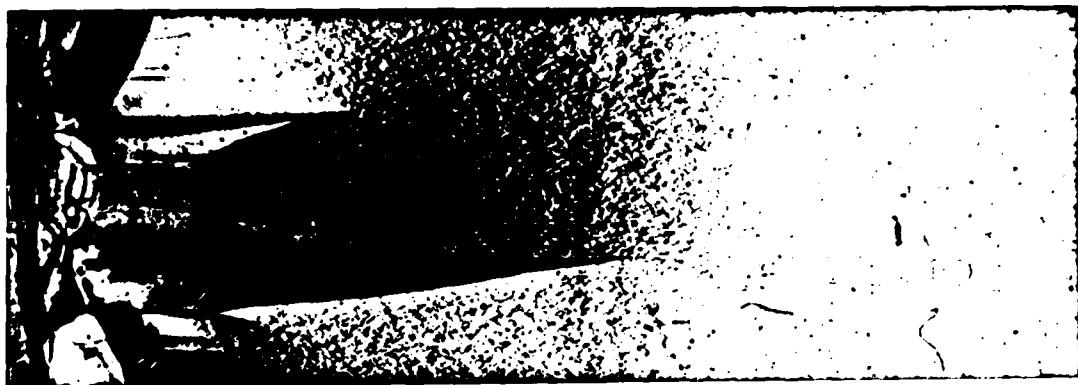
c) 100°C; 805 psi

Fig. 12   Crack Path Stability for Initial Crack
Propagation

SYMMETRIC

BRANCHING
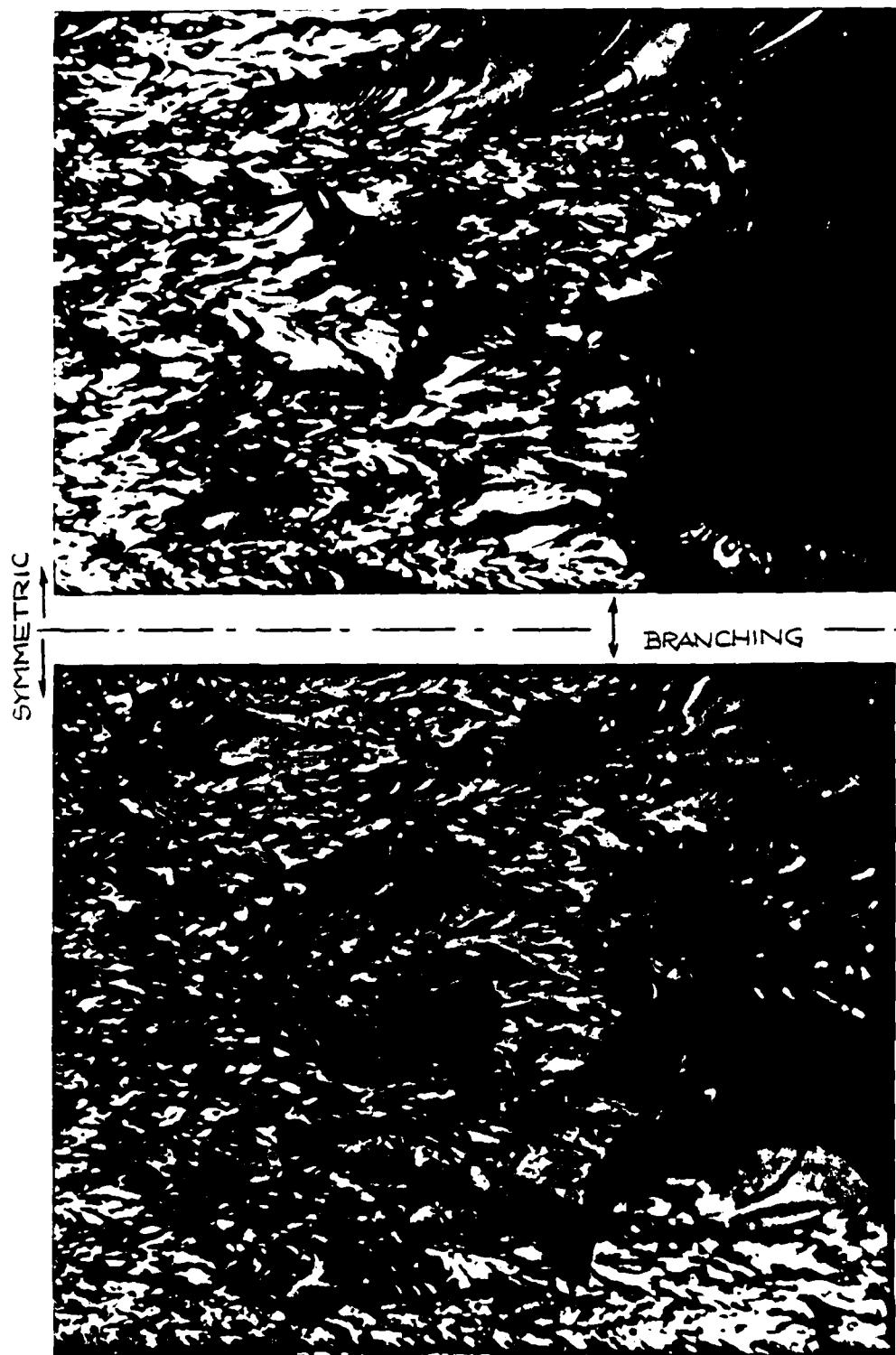
Fig. 13 Mating Fracture Surfaces Near Branch Location
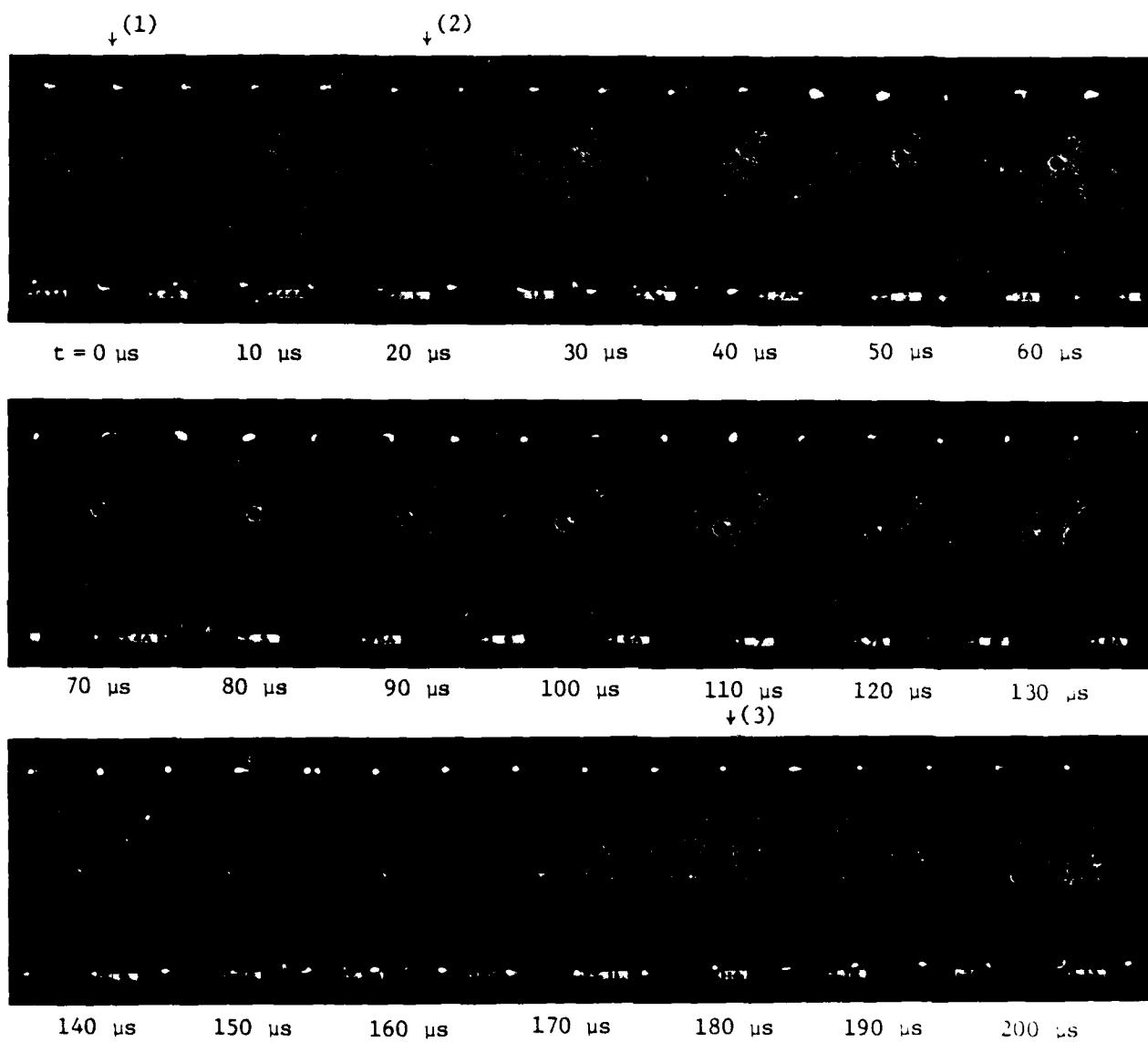
Fig. 14(a). Caustics for a running crack in Homalite-100: (1.) Stress-wave arrival; (2.) Initiation of running crack; (3.) Crack bifurcation. (Pictures taken with high-speed camera at California Institute of Technology.)
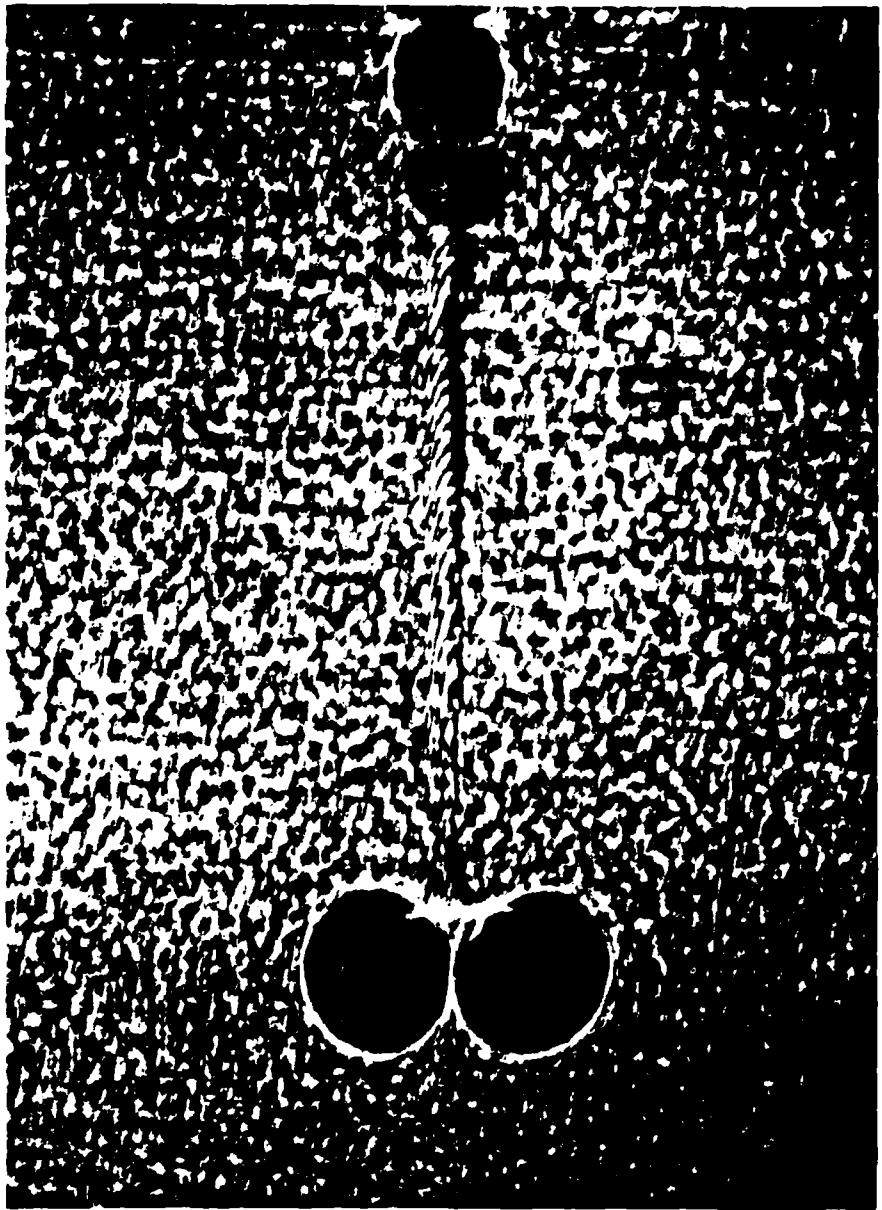
Fig. 14(b). Caustics, or shadow-spots, of a crack that has bifurcated (enlargement of frame in Fig. 5(a) at time t = 200 μs).
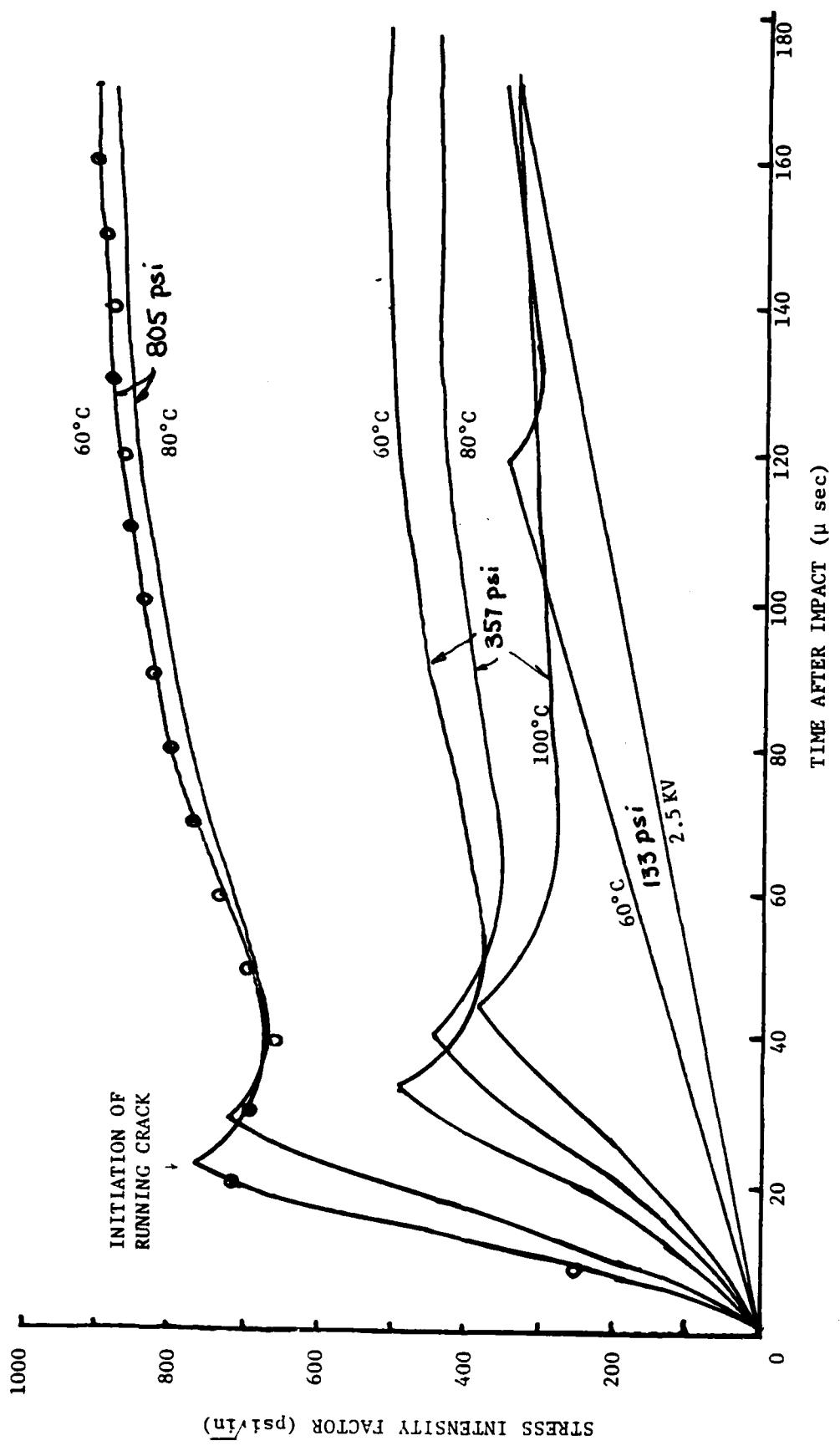
Fig. 14(c)Stress-intensity factor $K_I(t)$ as a function of time t for a running crack in Homalite-100.
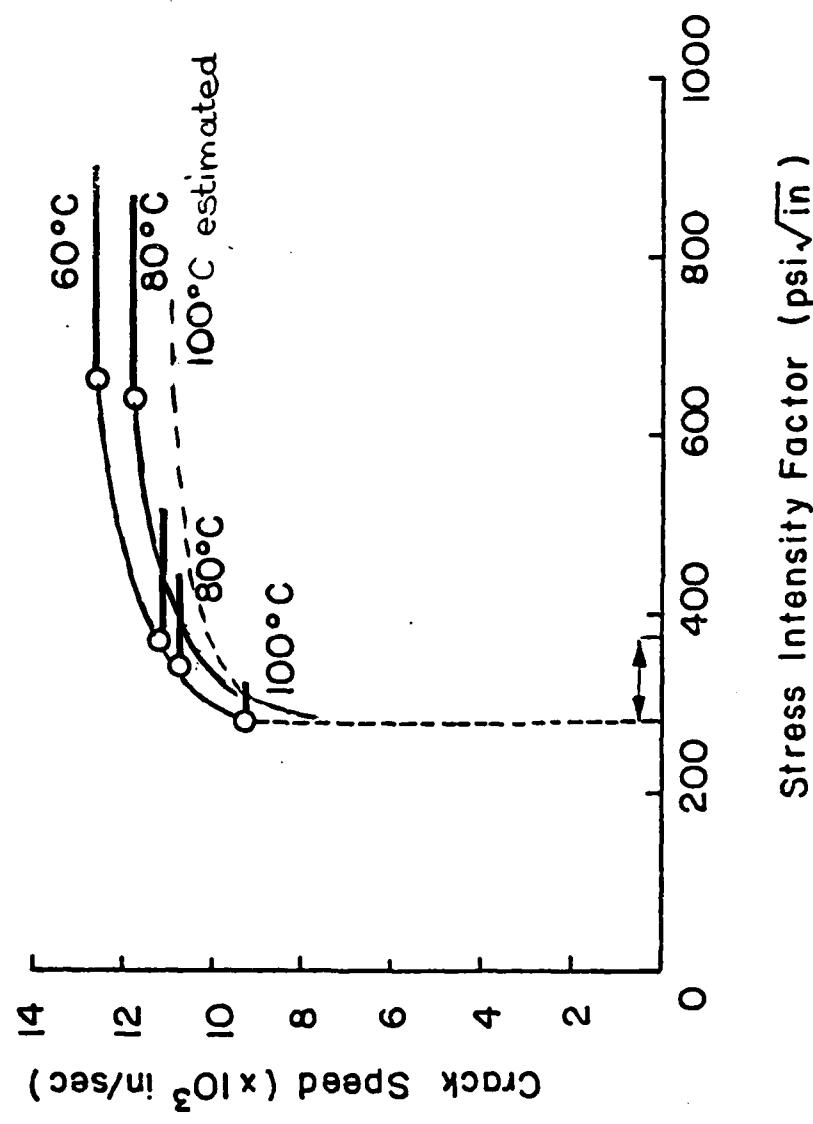
Fig. 15 Crack Speeds in Homalite 100
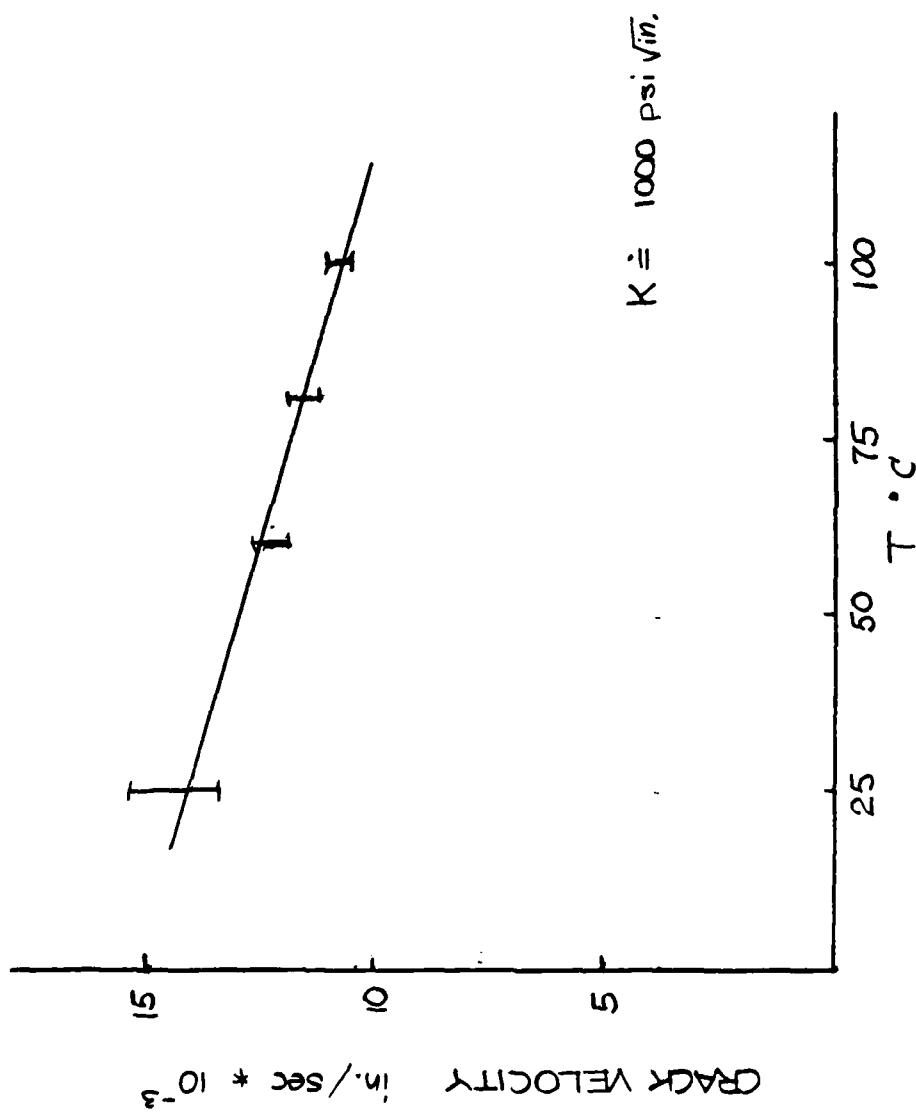
Fig. 16 Sensitivity of Crack Speed in Homalite 100
to Temperature
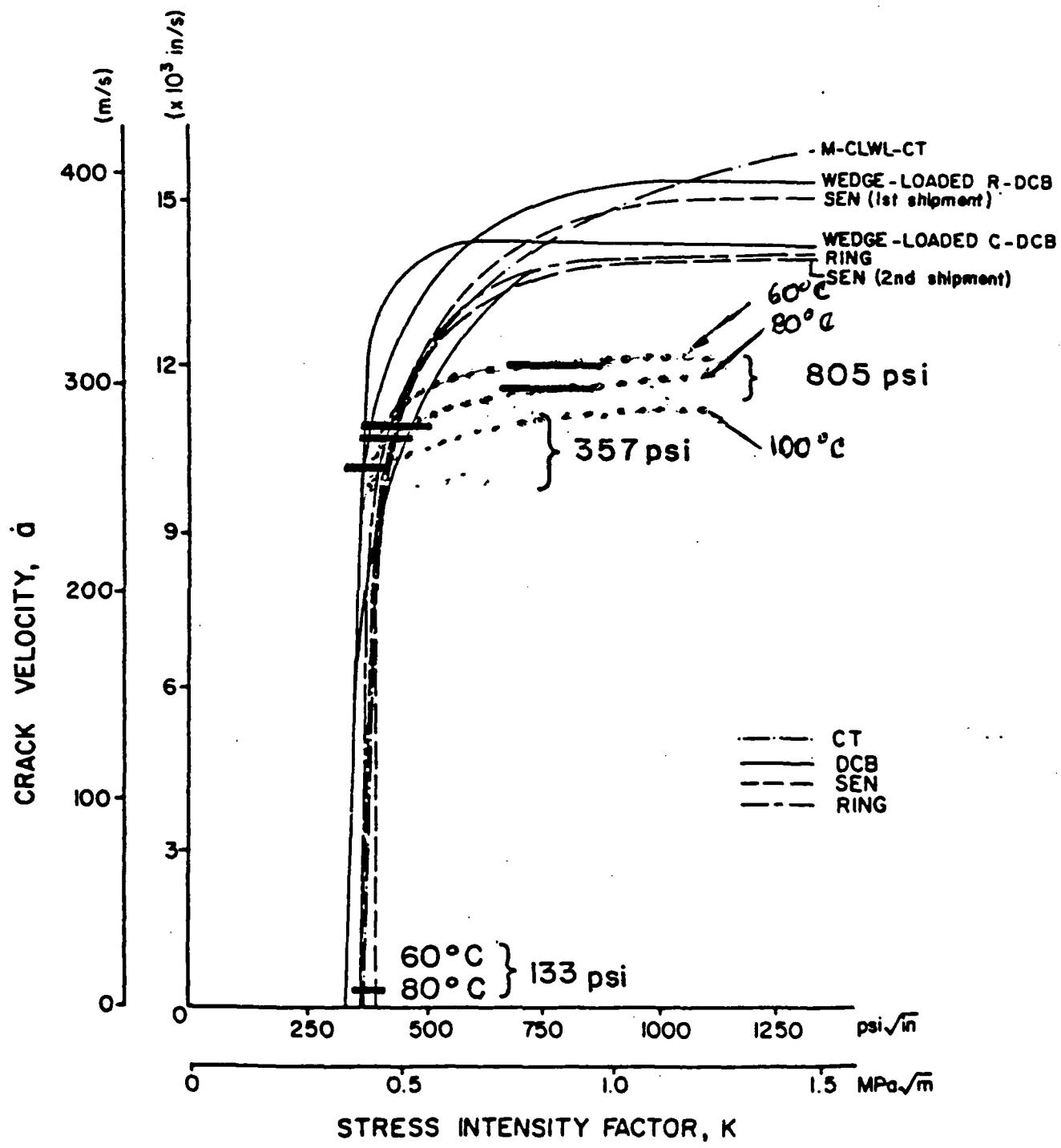
Fig. 17 Current Test Results Compared to those of other
Investigators.
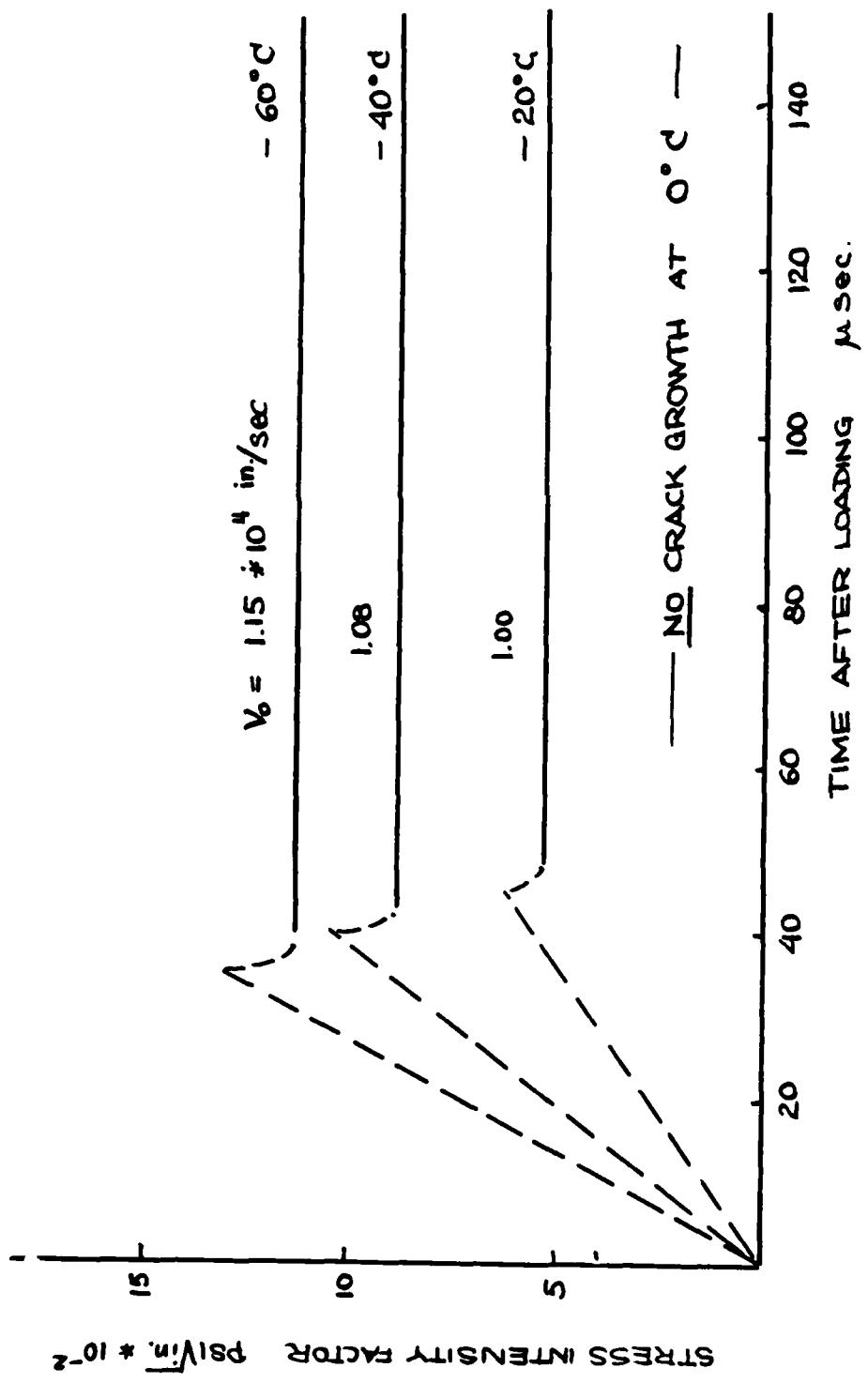
Fig. 18 Stress Intensity History in Solithane 113
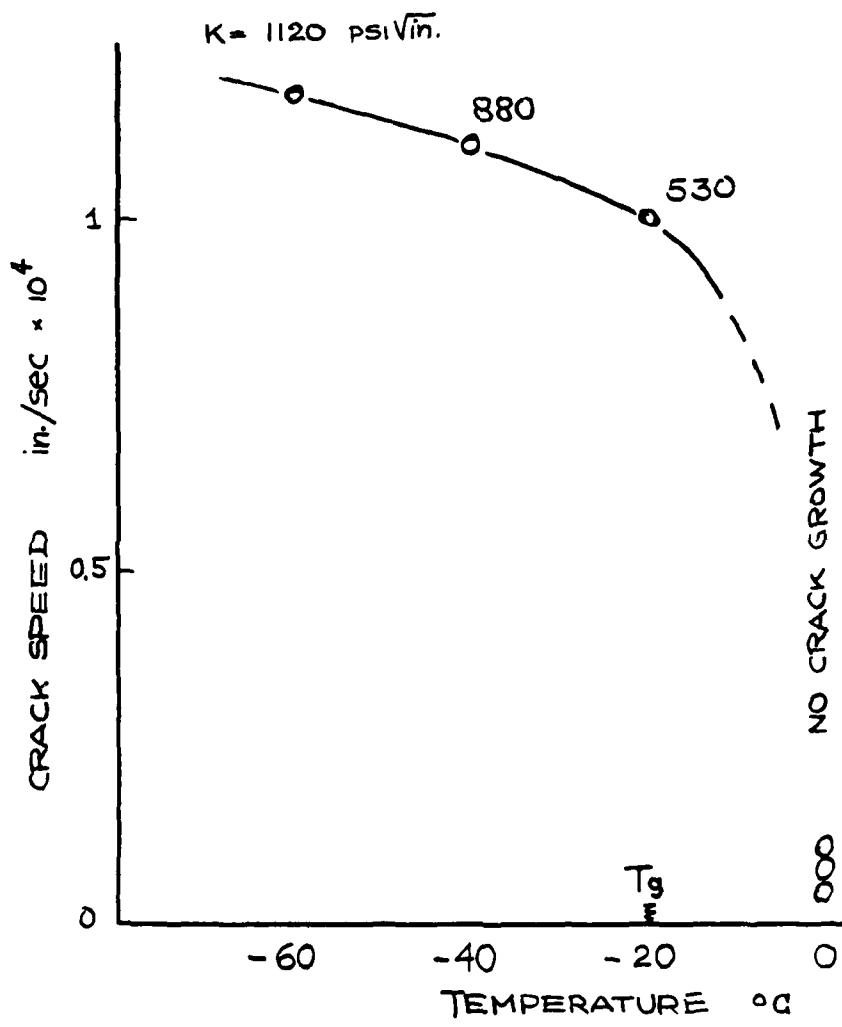
Fig. 19   Effect of Temperature on Crack Speeds in
          Solithane 113
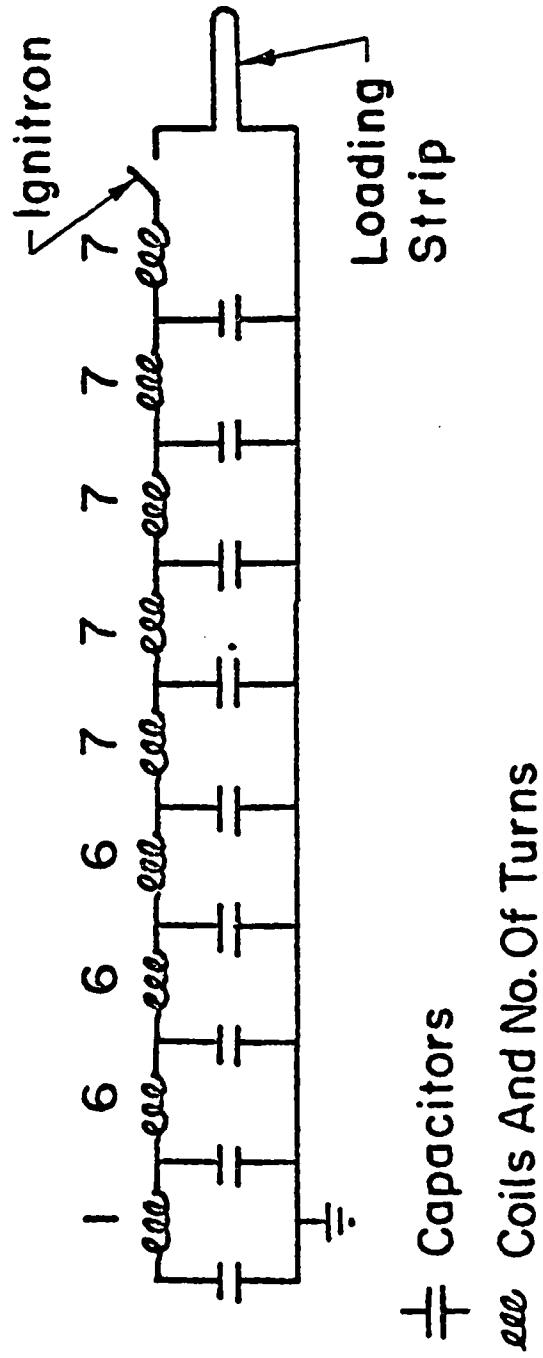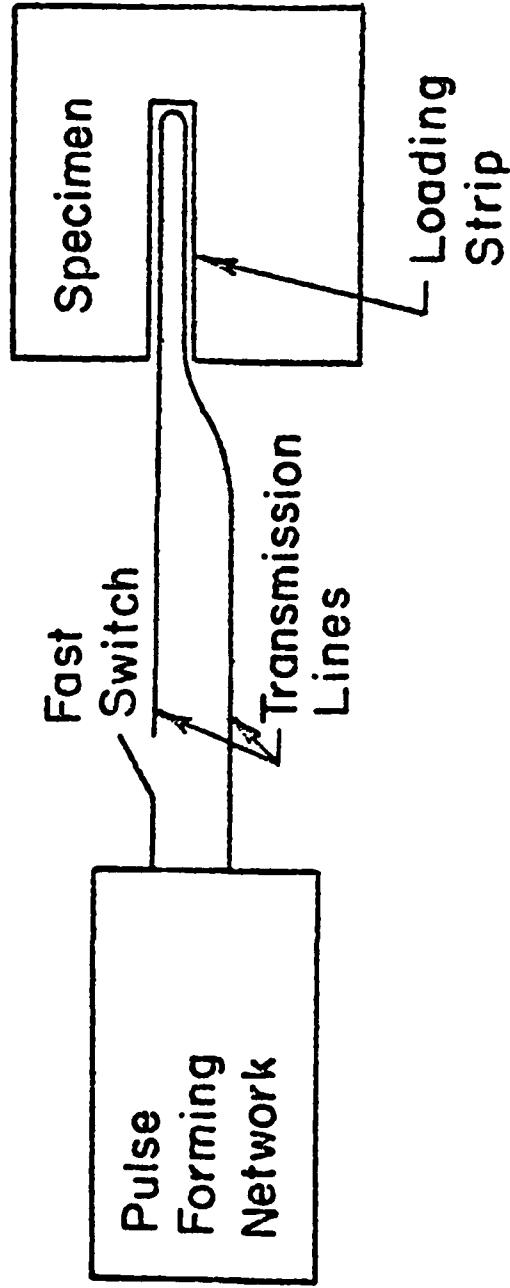
Fig. 20 Schematic of the Dynamic Loading Device
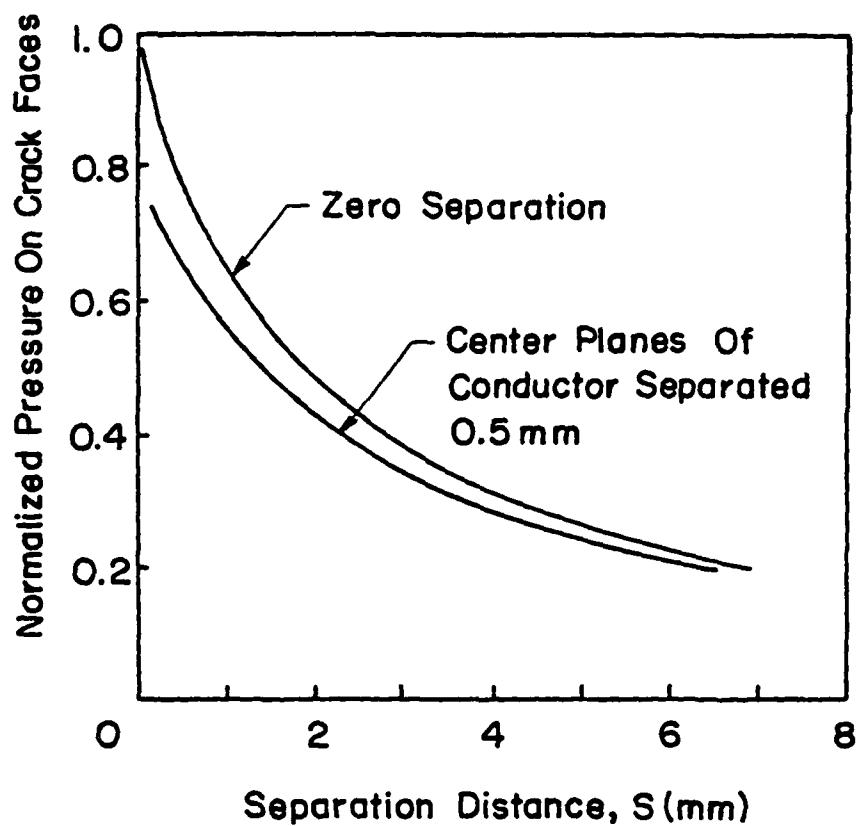
FIG.21 PRESSURE PRODUCED ON CRACK FACES
AS A FUNCTION OF STRIP SEPARATION

Fig. 22 Time Dependence of Crack Opening Displacement in Solithane 113 at 20°C
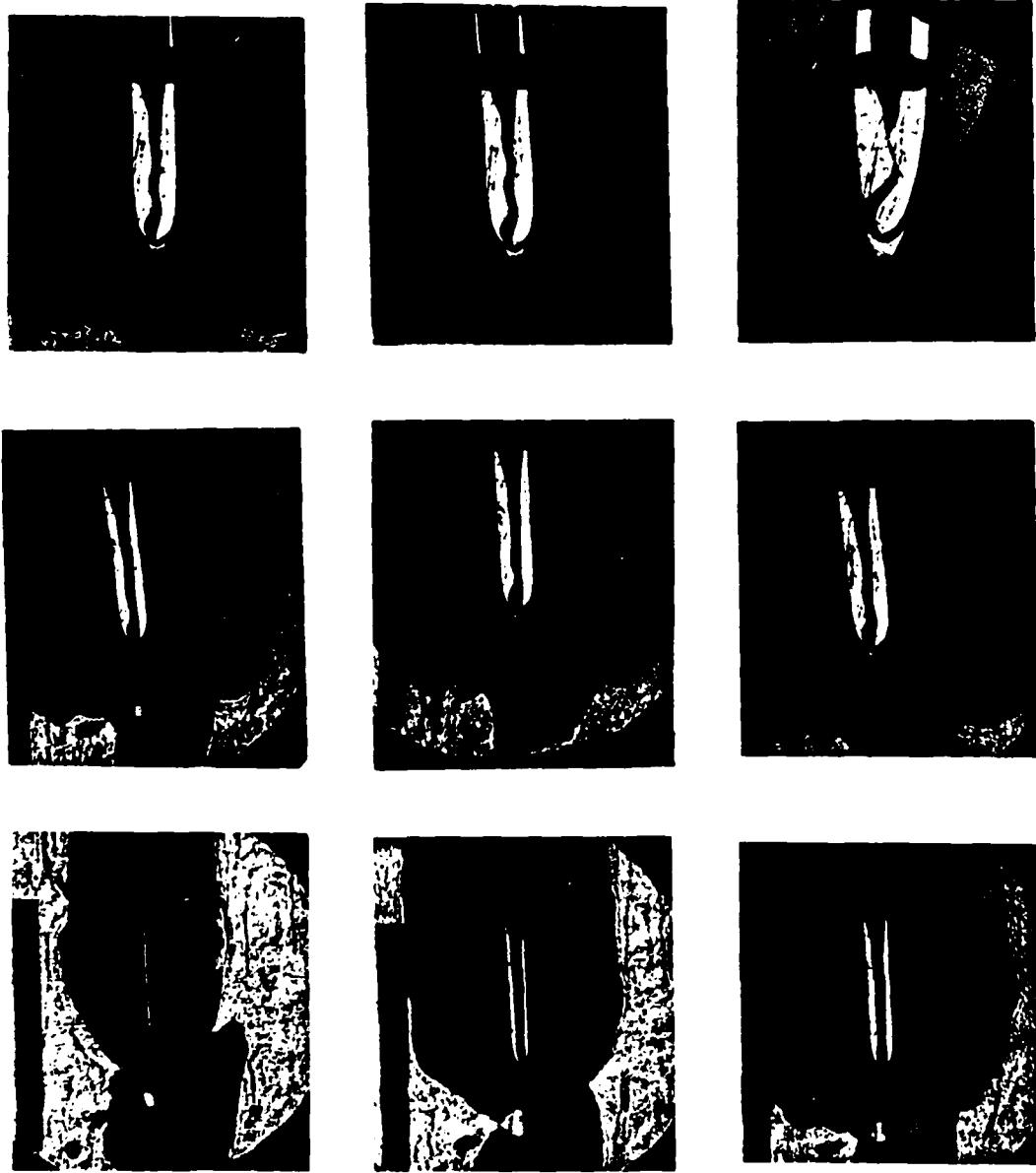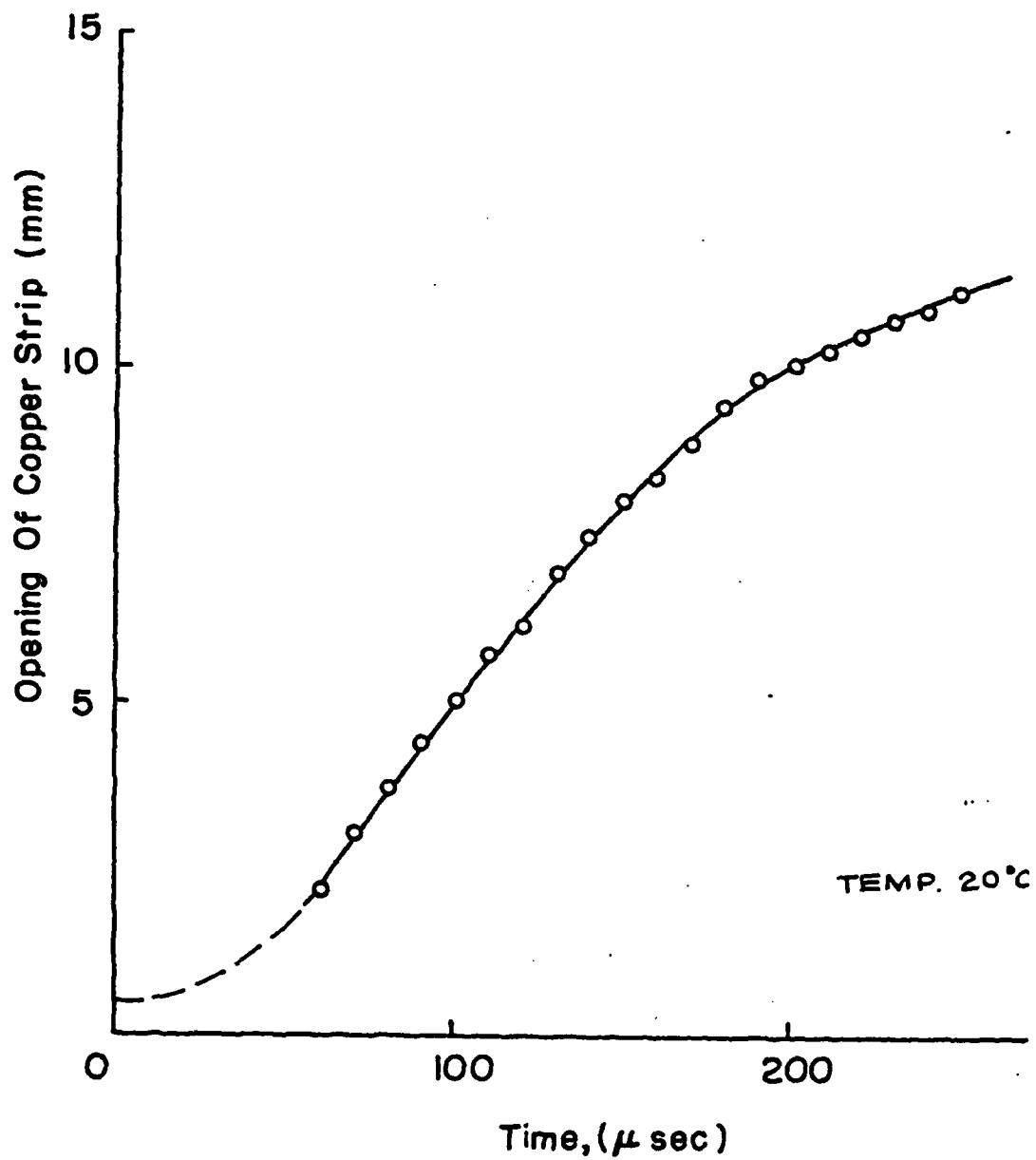
Fig. 23   Crack Opening Displacement vs time
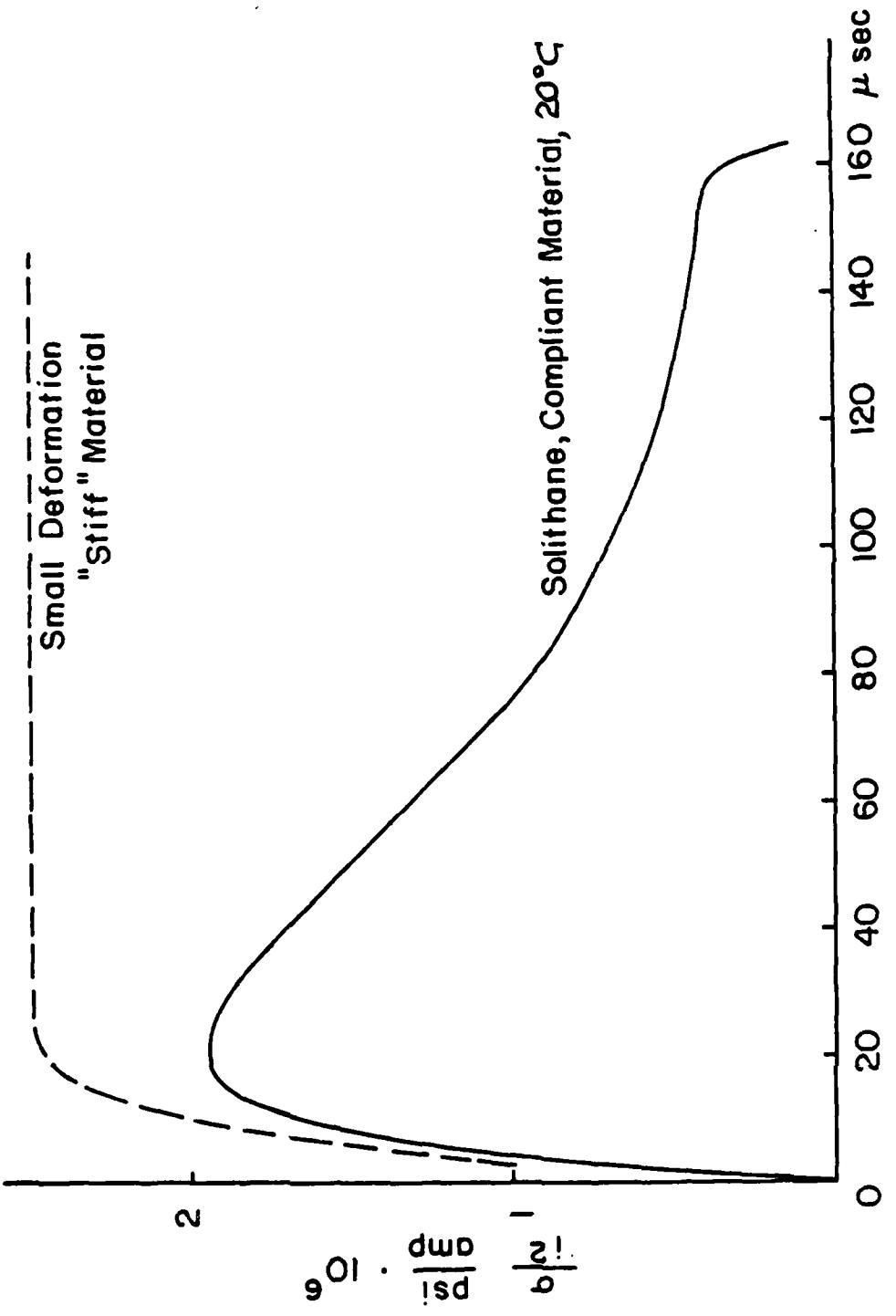
Fig. 24 Pressure Loss Attributed to Specimen Compliance
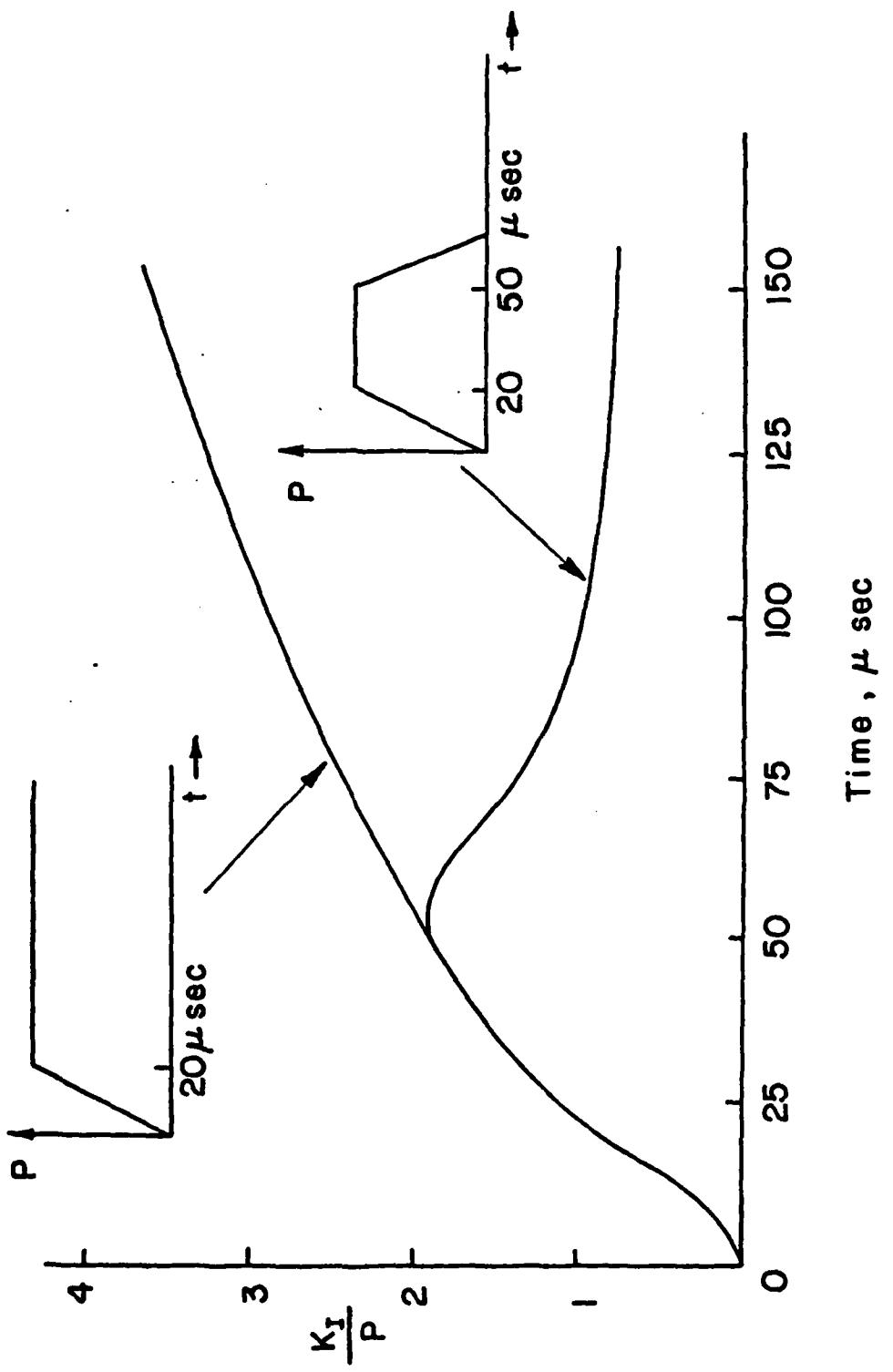
Fig. 25 Estimated Stress Intensity Factor Resulting from Pulse of Finite Duration
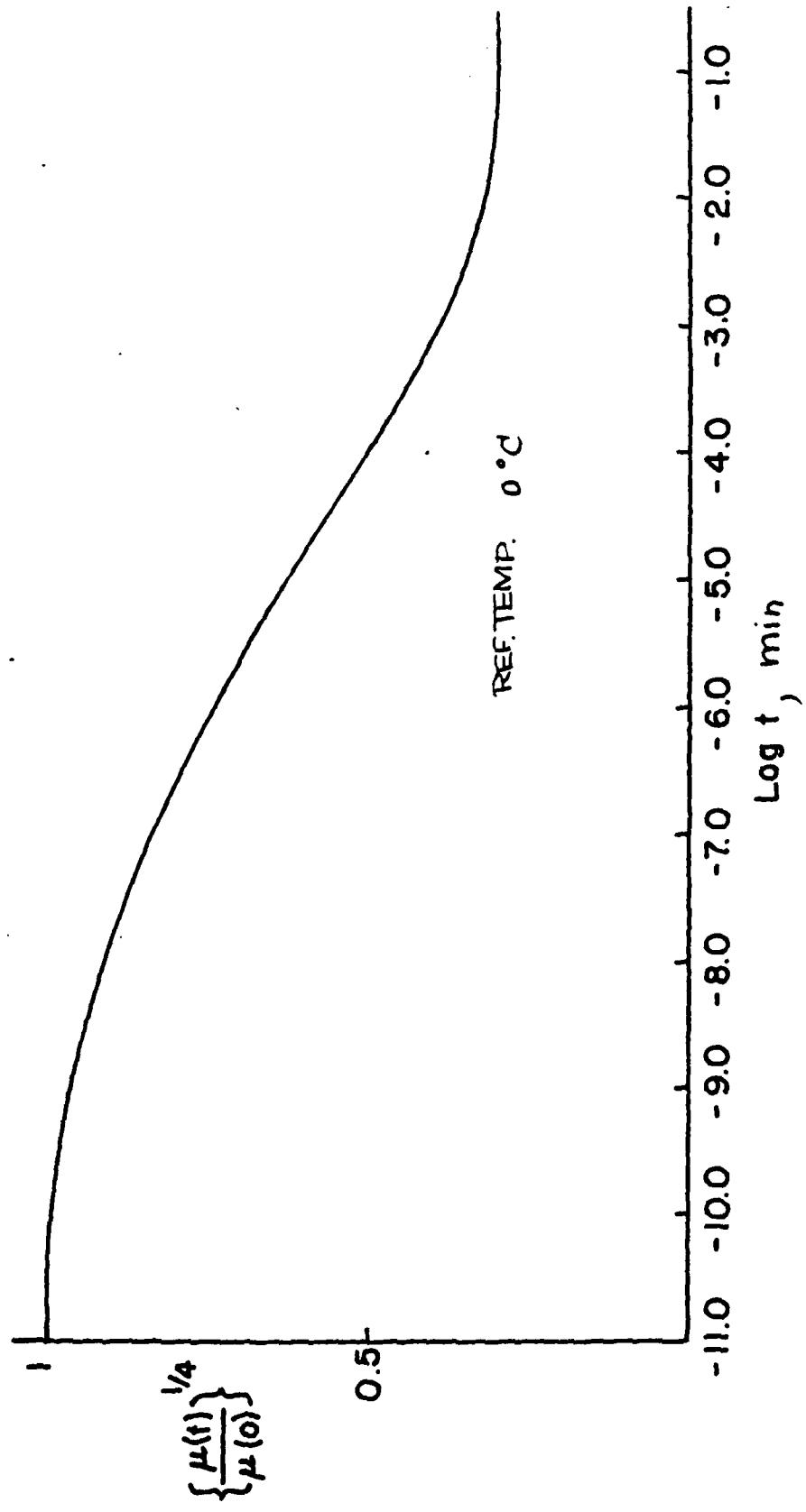
Fig. 26 Normalized Modulus Function at 0°C for
Solithane 113
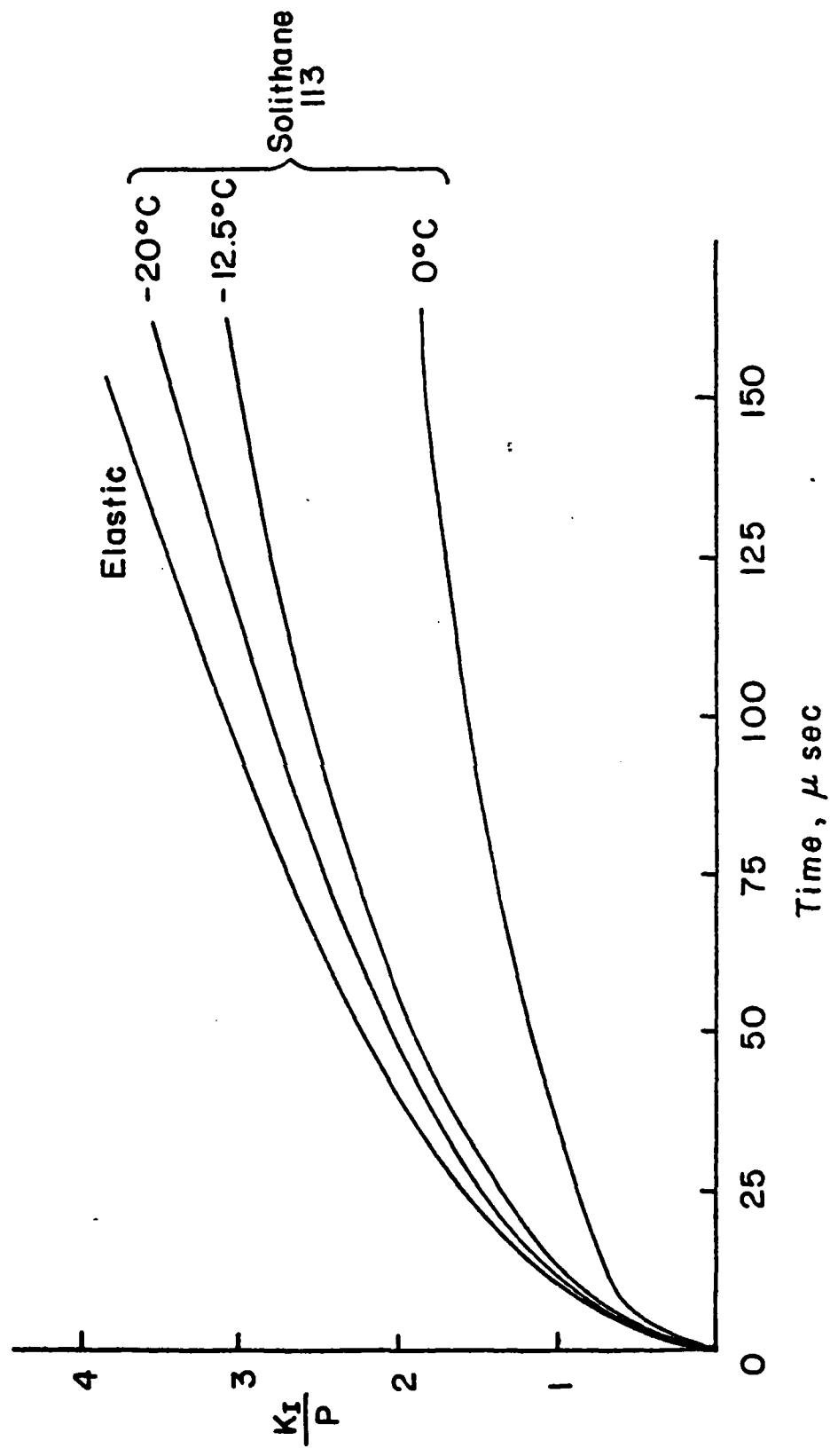
Fig. 27 Stress Intensity Factor for a Stationary Crack
at Different Temperatures

DISTRIBUTION LIST

|	No. Copies		No. Copies
Dr. L.V. Schmidt Assistant Secretary of the Navy (R,E, and S) Room 5E 731 Pentagon Washington, D.C. 20350	1	Dr. F. Roberto Code AFRPL MKPA Edwards AFB, CA 93523	1
Dr. A.L. Slafkosky Scientific Advisor Commandant of the Marine Corps Code RD-1 Washington, D.C. 20380	1	Dr. L.H. Caveny Air Force Office of Scientific Research Directorate of Aerospace Sciences Bolling Air Force Base Washington, D.C. 20332	1
Dr. Richard S. Miller Office of Naval Research Code 413 Arlington, VA 22217	10	Mr. Donald L. Ball Air Force Office of Scientific Research Directorate of Chemical Sciences Bolling Air Force Base Washington, D.C. 20332	1
Mr. David Siegel Office of Naval Research Code 260 Arlington, VA 22217	1	Dr. John S. Wilkes, Jr. FJSRL/NC USAF Academy, CO 80840	1
Dr. R.J. Marcus Office of Naval Research Western Office 1030 East Green Street Pasadena, CA 91106	1	Dr. R.L. Lou Aerojet Strategic Propulsion Co. P.O. Box 15699C Sacramento, CA 95813	1
Dr. Larry Peebles Office of Naval Research East Central Regional Office 666 Summer Street, Bldg. 114-D Boston, MA 02210	1	Dr. V.J. Keenan Anal-Syn Lab Inc. P.O. Box 547 Paoli, PA 19301	1
Dr. Phillip A. Miller Office of Naval Research San Francisco Area Office One Hallidie Plaza, Suite 601 San Francisco, CA 94102	1	Dr. Philip Howe Army Ballistic Research Labs ARRADCOM Code DRDAR-BLT Aberdeen Proving Ground, MD 21005	1
Mr. Otto K. Heiney AFATL - DLDL Elgin AFB, FL 32542	1	Mr. L.A. Watermeier Army Ballistic Research Labs ARRADCOM Code DRDAR-BLI Aberdeen Proving Ground, MD 21005	1
Mr. R. Geisler ATTN: MKP/MS24 AFRPL Edwards AFB, CA 93523	1	Dr. W.W. Wharton Attn: DRSMI-RKL Commander U.S. Army Missile Command Redstone Arsenal, AL 35898	1

DISTRIBUTION LIST

	No. Copies		No. Copies
Dr. R.G. Rhoades Commander Army Missile Command DRSMI-R Redstone Arsenal, AL 35898	1	Dr. E.H. Debutts Hercules Inc. Baccus Works P.O. Box 98 Magna, UT 84044	1
Dr. W.D. Stephens Atlantic Research Corp. Pine Ridge Plant 7511 Wellington Rd. Gainesville, VA 22065	1	Dr. James H. Thacher Hercules Inc. Magna Baccus Works P.O. Box 98 Magna, UT 84044	1
Dr. A.W. Barrows Ballistic Research Laboratory USA ARRADCOM DRDAR-BLP Aberdeen Proving Ground, MD 21005	1	Mr. Theordore M. Gilliland Johns Hopkins University APL Chemical Propulsion Info. Agency Johns Hopkins Road Laurel, MD 20810	1
Dr. C.M. Frey Chemical Systems Division P.O. Box 358 Sunnyvale, CA 94086	1	Dr. R. McGuire Lawrence Livermore Laboratory University of California Code L-324 Livermore, CA 94550	1
Professor F. Rodriguez Cornell University School of Chemical Engineering Olin Hall, Ithaca, N.Y. 14853	1	Dr. Jack Linsk Lockheed Missiles & Space Co. P.O. Box 504 Code Org. 83-10, Bldg. 154 Sunnyvale, CA 94088	1
Defense Technical Information Center DTIC-DDA-2 Cameron Station Alexandria, VA 22314	12	Dr. B.G. Craig Los Alamos National Lab P.O. Box 1663 NSP/DOD, MS-245 Los Alamos, NM 87545	1
Dr. Rocco C. Musso Hercules Aerospace Division Hercules Incorporated Alleghany Ballistic Lab P.O. Box 210 Washington, D.C. 21502	1	Dr. R.L. Rabie WX-2, MS-952 Los Alamos National Lab. P.O. Box 1663 Los Alamos NM 37545	1
Dr. Ronald L. Simmons Hercules Inc. Eglin AFATL/DLDL Eglin AFB, FL 32542	1	Dr. B. Rogers, WX-2 Los Alamos Scientific Lab. P.O. Box 1663 Los Alamos, NM 37545	1

DISTRIBUTION LIST

	No. Copies		No. Copies

Mr. R. Brown   1
Naval Air Systems Command
Code 330
Washington, D.C.   20361

Dr. J. Schnur   1
Naval Research Lab.
Code 6510
Washington, D.C.   20375

Dr. H. Rosenwasser   1
Naval Air Systems Command
AIR-310C
Washington, D.C.   20360

Mr. R. Beauregard   1
Naval Sea Systems Command
SEA 64E
Washington, D.C.   20362

Mr. B. Sobers   1
Naval Air Systems Command
Code 03P25
Washington, D.C.   20360

Mr. G. Edwards   1
Naval Sea Systems Command
Code 62R3
Washington, D.C.   20362

Dr. L.R. Rothstein   1
Assistant Director
Naval Explosives Dev.
Engineering Dept.
Naval Weapons Station
Yorktown, VA   23691

Mr. John Boyle   1
Materials Branch
Naval Ship Engineering Center
Philadelphia, PA   19112

Dr. H.G. Adolph   1
Naval Surface Weapons Center
Code R11
White Oak
Silver Spring, MD   20910

Dr. Lionel Dickinson   1
Naval Explosive Ordnance
Disposal Tech. Center
Code D
Indian Head, MD   20640

Dr. T.D. Austin   1
Naval Surface Weapons Center
Code R16
Indian Head, MD   20640

Mr. C.L. Adams   1
Naval Ordnance Station
Code PM4
Indian Head, MD   20640

Dr. T. Hall   1
Code R-11
Naval Surface Weapons Center
White Oak Laboratory
Silver Spring, MD   20910

Mr. S. Mitchell   1
Naval Ordnance Station
Code 5253
Indian Head, MO   20640

Mr. G.L. Mackenzie   1
Naval Surface Weapons Center
Code R101
Indian Head, MD   20640

Dr. William Tolles   1
Dean of Research
Naval Postgraduate School
Monterey, CA   93940

Dr. K.F. Mueller   1
Naval Surface Weapons Center
Code R11
White Oak
Silver Spring, MD   20910

Naval Research Lab.   1
Code 6100
Washington, D.C.   20375

DISTRIBUTION LIST

	No. Copies		No. Copies
Mr. J. Murrin Naval Sea Systems Command Code 62R2 Washington, D.C. 20362	1	Dr. A. Nielsen Naval Weapons Center Code 385 China Lake, CA 93555	1
Dr. D.J. Pastine Naval Surface Weapons Cneter Code R04 White Oak Silver Spring, MD 20910	1	Dr. R. Reed, Jr. Naval Weapons Center Code 388 China Lake, CA 93555	1
Mr. L. Roslund Naval Surface Weapons Center Code R122 White Oak, Silver Spring MD 20910	1	Dr. L. Smith Naval Weapons Center Code 3205 China Lake, CA 93555	1
Mr. M. Stosz Naval Surface Weapons Center Code R121 White Oak Silver Spring, MD 20910	1	Dr. B. Douda Naval Weapons Support Center Code 5042 Crane, Indiana 47522	1
Dr. E. Zimmet Naval Surface Weapons Center Code R13 White Oak Silver Spring, MD 20910	1	Dr. A. Faulstich Chief of Naval Technology MAT Code 0716 Washington, D.C. 20360	1
Dr. D. R. Derr Naval Weapons Center Code 388 China Lake, CA 93555	1	LCDR J. Walker Chief of Naval Material Office of Naval Technology MAT, Code 0712 Washington, D.C. 20360	1
Mr. Lee N. Gilbert Naval Weapons Center Code 3205 China Lake, CA 93555	1	Mr. Joe McCartney Naval Ocean Systems Center San Diego, CA 92152	1
Dr. E. Martin Naval Weapons Center Code 3858 China Lake, CA 93555	1	Dr. S. Yamamoto Marine Sciences Division Naval Ocean Systems Center San Diego, CA 91232	1
Mr. R. McCarten Naval Weapons Center Code 3272 China Lake, CA 93555	1	Dr. G. Bosmajian Applied Chemistry Division Naval Ship Research & Development Center Annapolis, MD 21401	1
		Dr. H. Shuey Rohn and Haas Company Huntsville, Alabama 35801	1

DISTRIBUTION LIST

<div align="center">No. Copies   No. Copies</div>

Dr. J.F. Kincaid   1
Strategic Systems Project
Office
Department of the Navy
Room 901
Washington, D.C. 20376

Strategic Systems Project Office   1
Propulsion Unit
Code SP2701
Department of the Navy
Washington, D.C. 20376

Mr. E.L. Throckmorton   1
Strategic Systems Project Office
Department of the Navy
Room 1043
Washington, D.C. 20376

Dr. D.A. Flanigan   1
Thiokol
Huntsville Division
Huntsville, Alabama 35807

Mr. G.F. Mangum   1
Thiokol Corporation
Huntsville Division
Huntsville, Alabama 35807

Mr. E.S. Sutton   1
Thiokol Corporation
Elkton Division
P.O. Box 241
Elkton, MD 21921

Dr. G. Thompson   1
Thiokol
Wasatch Division
MS 240 P.O. Box 524
Brigham City, UT 84302

Dr. T.F. Davidson   1
Technical Director
Thiokol Corporation
Government Systems Group
P.O. Box 9258
Ogden, Utah 84409

Dr. C.W. Vriesen   1
Thiokol Elkton Division
P.O. Box 241
Elkton, MD 21921

Dr. J.C. Hinshaw   1
Thiokol Wasatch Division
P.O. Box 524
Brigham City, Utah 83402

U.S. Army Research Office   1
Chemical & Biological Sciences
Division
P.O. Box 12211
Research Triangle Park
NC 27709

Dr. R.F. Walker   1
USA ARRADCOM
DRDAR-LCE
Dover, NJ 07801

Dr. T. Sinden   1
Munitions Directorate
Propellants and Explosives
Defence Equipment Staff
British Embassy
3100 Massachusetts Ave.
Washington, D.C. 20008

LTC B. Loving   1
AFROL/LK
Edwards AFB, CA 93523

Professor Alan N. Gent   1
Institute of Polymer Science
University of Akron
Akron, OH 44325

Mr. J. M. Frankle   1
Army Ballistic Research Labs
ARRADCOM
Code DRDAR-BLI
Aberdeen Proving Ground, MD 21005

DISTRIBUTION LIST

No. Copies   No. Copies

Dr. Ingo W. May   1   Dr. J. P. Marshall   1
Army Ballistic Research Labs   Dept. 52-35, Bldg. 204/2
ARRADCOM   Lockheed Missile & Space Co.
Code DRDAR-BLI   3251 Hanover Street
Aberdeen Proving Ground, MD 21005   Palo Alto, CA 94304

Professor N.W. Tschoegl   1   Ms. Joan L. Janney   1
California Institute of Tech   Los Alamos National Lab
Dept. of Chemical Engineering   Mail Stop 920
Pasadena, CA 91125   Los Alamos, NM 87545

Professor M.D. Nicol   1   Dr. J. M. Walsh   1
University of California   Los Alamos Scientific Lab
Dept. of Chemistry   Los Alamos, NM 87545
405 Hilgard Avenue
Los Angeles, CA 90024   Professor R. W. Armstrong   1
                                          Univ. of Maryland
Professor A. G. Evans   1   Department of Mechanical Eng.
University of California   College Park, MD 20742
Berkeley, CA 94720
                                          Prof. Richard A. Reinhardt   1
Professor T. Litovitz   1   Naval Postgraduate School
Catholic Univ. of America   Physics & Chemistry Dept.
Physics Department   Monterey, CA 93940
520 Michigan Ave., N.E.
Washington, D.C. 20017   Dr. R. Bernecker   1
                                          Naval Surface Weapons Center
Professor W. G. Knauss   1   Code R13
Graduate Aeronautical Lab   White Oak, Silver Spring, MD 20910
California Institute of Tech.
Pasadena, CA 91125   Dr. M. J. Kamlet   1
                                          Naval Surface Weapons Center
Professor Edward Price   1   Code R11
Georgia Institute of Tech.   White Oak, Silver Spring, MD 20910
School of Aerospace Engin.
Atlanta, Georgia 30332   Professor J. D. Achenbach   1
                                          Northwestern University
Dr. Kenneth O. Hartman   1   Dept. of Civil Engineering
Hercules Aerospace Division   Evanston, IL 60201
Hercules Incorporated
P.O. Box 210   Dr. N. L. Basdekas   1
Cumberland, MD 21502   Office of Naval Research
                                          Mechanics Program, Code 432
Dr. Thor L. Smith   1   Arlington, VA 22217
IBM Research Lab
D42.282   Professor Kenneth Kuo   1
San Jose, CA 95193   Pennsylvania State Univ.
                                          Dept. of Mechanical Engineering
                                          University Park, PA 16802

DISTRIBUTION LIST

	No. Copies		No. Copies

Dr. S. Sheffield   1
Sandia Laboratories
Division 2513
P.O. Box 5800
Albuquerque, NM 87185 ·

Dr. M. Farber   1
Space Sciences, Inc.
135 Maple Avenue
Monrovia, CA 91016

Dr. Y. M. Gupta   1
SRI International
333 Ravenswood AVenue
Menlo Park, CA 94025

Mr. M. Hill   1
SRI International
333 Ravenswood Avenue
Menlo Park, CA 94025

Professor Richard A. Schapery   1
Texas A&M Univ.
Dept of Civil Engineering
College Station, TX 77843

Dr. Stephen Swanson   1
Univ. of Utah
Dept. of Mech. & Industrial
    Engineering
MEB 3008
Salt Lake City, UT 84112

Mr. J. D. Byrd   1
Thiokol Corp. Huntsville
Huntsville Div.
Huntsville, AL 35807

Professor G. D. Duvall   1
Washington State University
Dept. of Physics
Pullman, WA 99163

Prof. T. Dickinson   1
Washington State University
Dept. of Physics
Pullman, WA 99163

Rockwell International   1
12214 Lakewood Blvd.
Downey, CA 90241
Attn: H.M. Clancy,
     Mail Stop AB 70

ONR Resident Representative 1
Ohio State University
Research Center
1314 Kinnear Road
Columbus, Ohio 43212
Attn: Joseph Haggard,
     Dept. of the Navy